การรับแรงพลวัตร่วมกันระหว่างแผ่นพื้นสี่เหลี่ยมและตัวกลางโพโรอิลาสติกหลายชั้น

นายรวิภาส แปลงมาลย์

วิทยานิพนธ์นี้เป็นส่วนหนึ่งของการศึกษาตามหลักสูตรปริญญาวิศวกรรมศาสตรมหาบัณฑิต
สาขาวิชาวิศวกรรมโยธา ภาควิชาวิศวกรรมโยธา
คณะวิศวกรรมศาสตร์ จุฬาลงกรณ์มหาวิทยาลัย
ปีการศึกษา 2559

DYNAMIC INTERACTION BETWEEN RECTANGULAR PLATE AND MULTI-LAYERED POROELASTIC MEDIA

Mr. Rawiphas Plangmal

A Thesis Submitted in Partial Fulfillment of the Requirements
for the Degree of Master of Engineering Program in Civil Engineering
Department of Civil Engineering
Faculty of Engineering
Chulalongkorn University
Academic Year 2016

Thesis Title	DYNAMIC INTERACTION BETWEEN RECTANGULAR PLATE AND MULTI-LAYERED POROELASTIC MEDIA
By	Mr. Rawiphas Plangmal
Field of Study	Civil Engineering
Thesis Advisor	ProfessorTeerapong Senjuntichai, Ph.D.

Accepted by the Faculty of Engineering, Chulalongkorn University in Partial Fulfillment of the Requirements for the Master's Degree

.....Dean of the Faculty of Engineering
(Associate Professor Supot Teachavorasinskun, Ph.D.)

THESIS COMMITTEE

.....Chairman
(Associate ProfessorJaroon Rungamornrat, Ph.D.)
.....Thesis Advisor
(ProfessorTeerapong Senjuntichai, Ph.D.)
.....External Examiner
(Pong-in Intarit, Ph.D.)

รวิภาส แปลงมาลย์ : การรับแรงพลวัตร่วมกันระหว่างแผ่นพื้นสี่เหลี่ยมและตัวกลางโพโรอิลาสติกหลายชั้น (DYNAMIC INTERACTION BETWEEN RECTANGULAR PLATE AND MULTI-LAYERED POROELASTIC MEDIA) อ.ที่ปรึกษาวิทยานิพนธ์หลัก: ศ. ดร.ธีรพงศ์ เสนจันทร์ฒิไชย, 63 หน้า.

วิทยานิพนธ์ฉบับนี้นำเสนอปัญหาการรับแรงพลวัตร่วมกันระหว่างแผ่นพื้นสี่เหลี่ยมกับตัวกลางโพโรอิลาสติกหลายชั้น โดยสมมุติให้พฤติกรรมของแผ่นพื้นสี่เหลี่ยมมีการเคลื่อนที่แบบวัตถุแข็งเกร็งภายใต้แรงกระทำ และให้น้ำสามารถซึมผ่านได้บริเวณผิวสัมผัสระหว่างแผ่นพื้นและตัวกลางโพโรอิลาสติก งานวิจัยนี้ใช้วิธีสติฟเนสแม่นตรงในการแก้ปัญหาตัวกลางโพโรอิลาสติกหลายชั้นซึ่งมีพฤติกรรมเป็นไปตามทฤษฎีของ Biot พื้นที่ผิวสัมผัสระหว่างแผ่นพื้นสี่เหลี่ยมและตัวกลางโพโรอิลาสติกได้ถูกแบ่งย่อยออกเป็นชิ้นส่วนสี่เหลี่ยมเล็กๆจำนวนหลายชิ้นและสมมุติให้แรงที่ไม่ทราบค่าภายในแต่ละชิ้นส่วนย่อยมีค่าคงที่ ระบบสมการได้ถูกสร้างขึ้นจากคำตอบที่ได้จากวิธีสติฟเนสแม่นตรงเพื่อคำนวณหาแรงในแต่ละชิ้นส่วนย่อย วิทยานิพนธ์ฉบับนี้ได้ทำการพิจารณาแผ่นพื้นสี่เหลี่ยมภายใต้แรงกระทำในแนวดิ่ง,แนวราบ,แรงดัด และแรงบิด ผลการศึกษาที่นำเสนอในวิทยานิพนธ์แสดงให้เห็นถึงอิทธิพลของตัวแปรต่างๆได้แก่ ระยะฝังของแผ่นพื้นสี่เหลี่ยม, ความถี่ของแรงกระทำ, อัตราส่วนความกว้างต่อความยาวของแผ่นพื้น และช่องเปิดในแผ่นพื้นสี่เหลี่ยม ที่มีต่อพฤติกรรมการรับแรงพลวัตร่วมกันระหว่างแผ่นพื้นสี่เหลี่ยมกับตัวกลางโพโรอิลาสติกหลายชั้น

ภาควิชา วิศวกรรมโยธา ลายมือชื่อนิสิต .....

สาขาวิชา วิศวกรรมโยธา ลายมือชื่อ อ.ที่ปรึกษาหลัก .....

ปีการศึกษา 2559

5770282121 : MAJOR CIVIL ENGINEERING
KEYWORDS:

RAWIPHAS PLANGMAL: DYNAMIC INTERACTION BETWEEN RECTANGULAR PLATE AND MULTI-LAYERED POROELASTIC MEDIA. ADVISOR: PROF.TEERAPONG SENJUNTICHAI, Ph.D., 63 pp.

This thesis is concerned with dynamic interaction between a rectangular plate and a multi-layered poroelastic medium. The plate is assumed to be massless and rigid, and subjected to time-harmonic vertical, horizontal, and moment loading. In addition, the contact area between the plate and the supporting medium is assumed to be fully permeable. The poroelastic medium under consideration consists of *N* poroelastic layers of different thicknesses and material properties, and each layer is governed by Biot's poroelastodynamics theory. The interaction problem is formulated by dividing the contact area into a finite number of small rectangular elements with uniform traction distribution. Nodal points are selected at the center of each element. An equation system is formed to determine the magnitude of contact traction at the nodal points by imposing appropriate rigid body displacement boundary conditions. The influence functions required to establish the flexibility equation system correspond to the displacement of a multi-layered half-space under vertical and horizontal loads of unit intensity. These influence functions are obtained by employing the exact stiffness matrix method. A computer program based on the present numerical scheme has been developed, and the accuracy of the solution scheme has been confirmed by comparing with existing solutions. Selected numerical results are presented to demonstrate the influence of various parameters such as poroelastic material parameters, frequency of excitation, embedded depth, plate aspect ratio etc., on the compliances of a rigid rectangular plate.

Department:	Civil Engineering	Student's Signature	.....
Field of Study:	Civil Engineering	Advisor's Signature	.....
Academic Year:	2016		

ACKNOWLEDGEMENTS

The author wishes to express his sincere gratitude to his thesis advisor, Professor Dr.Teerapong Senjuntichai for his invaluable advices, encouragement and help throughout the course of this research. He would also like to thank his committee members, Associate Professor Dr. Jaroon Rungamornrat and Dr. Pong-in Intarit for providing useful comments and suggestions.

Special thanks are also due to his friends at the Department of Civil Engineering, Chulalongkorn University for helping directly and indirectly in the preparation of this thesis.

Finally, the author would like to express his appreciation to his family members for their continuous supports and encouragement.

CONTENTS

Page

LIST OF TABLES

LIST OF FIGURES

LIST OF SYMBOLS

a	a half of length of plate in $x-$direction;
A	a half of length of plate in $y-$direction;
b	parameter accounting for the internal friction of the medium;
C_{hh}	the horizontal compliance;
C_{hm}	the coupling compliance;
C_{mm}	the rocking compliance;
C_{tt}	the torsion compliance;
C_{vv}	the vertical compliance;
e	dilatation of the solid matrix;
F_i	external loading in $i-$direction;
G_{ij}	the displacement in $i-$direction due to loading $j-$direction;
H	Heaviside function;
$\mathbf{K}^{(n)}$	stiffness matrix of the nth layer;
K_{hh}	the horizontal impedance;
K_{hm}	the coupling impedance;
K_{mm}	the rocking impedance;
K_{tt}	the torsion impedance;
K_{vv}	the vertical impedance;
k_x	wave number along the $x-$axis;
k_y	wave number along the $y-$axis;
M	Biot 's parameters accounting for compressibility of the medium;
M_i	external moment in $i-$direction;
m	Biot 's density-like parameter;
N_x	number of element of plate in $x-$direction;
N_y	number of element of plate in $y-$direction;

p	excess pore pressure;
$\bar{Q}^{(n)}$	fluid source at nth layer interface;
$\bar{T}_i^{(n)}$	contact stress at the nth interface layered;
$\mathbf{t}^{(n)}$	external force at the nth interface layered;
t	time variable;
$\mathbf{u}^{(n)}$	generalized displacement vector for the nth layer;
u_i	displacement of the solid matrix in the $i-$direction;
w_i	fluid displacement relative to the solid matrix in the $i-$direction;
x	horizontal coordinate;
y	horizontal coordinate;
z	vertical coordinate;
α	Biot 's parameters accounting for compressibility of the medium;
δ	non-dimensional frequency;
δ_{ij}	Kronecker delta;
ε_{ij}	strain component of the solid matrix;
ζ	variation of fluid volume;
λ	Lame' constant of the bulk material;
μ	shear modulus of the bulk material;
v	Poisson 's ratio;
ρ	mass density of the bulk material;
ρ_f	mass density of the pore fluid;
$\boldsymbol{\sigma}^{(n)}$	generalized force vector for the nth layer;
σ_{ij}	total stress component of the bulk material;
Δ_i	the translation displacement in $i-$direction;
θ_i	the rotation displacement in $i-$direction;
ω	frequency domain;

Chapter 1
INTRODUCTION

1.1 General

The study of dynamic interaction between foundations and supporting soil medium has important applications in various civil engineering problems such as in the analysis and design of pavement, shallow and deep foundations. In the past, studies related to this dynamic interaction problem usually considered the supporting soil medium as a homogeneous elastic solid. However, geomaterials are often two-phased materials consisting of a solid skeleton with voids filled with fluid. These types of materials are commonly known as poroelastic materials, and are considered to be more realistic representation of soils and rocks than ideal elastic materials. In addition, natural soil profiles are generally layered in character. It is then more appropriate to consider the supporting soli medium as a multi-layered poroelastic half-space for this interaction problem. A review of literature indicates that dynamic interaction between rectangular plate and multi-layered poroelastic half-space has never been considered in the past.

Dynamic response of a rectangular plate embedded in multi-layered poroelastic media is investigated in this thesis. The plate is assumed to be massless and rigid, and subjected to time-harmonic vertical, horizontal, and moment loading. The poroelastic medium under consideration consists of *N* layers of different thicknesses and material properties, and is governed by Biot's poroelastodynamics theory. To investigate this interaction problem, the contact area between a rectangular plate and a poroelastic half-space is divided into a finite number of small rectangular elements with uniform traction distribution. Nodal points are selected at the center of each element. An equation system is set up to determine the magnitudes of unknown contact traction at different nodal points by applying appropriate rigid body displacement boundary conditions. The influence functions, required to establish the flexibility equation system, correspond to the displacements of a multi-layered half-space subjected to uniform vertical and horizontal loads, of unit intensity, applied over each discretized sub-region. These influence functions are obtained by employing the exact stiffness matrix method. In this

method, the stiffness matrix for each poroelastic layer is derived explicitly by applying the double-dimensional Fourier transformation with respect to the horizontal coordinates. The global stiffness equation of the layered system is then obtained by considering the continuity of traction and fluid flow at each layer interface. The solutions of the flexibility equation system and the equilibrium of forces result in the solutions for compliances of a rigid plate. A computer program based on the proposed scheme has been developed, and the accuracy of the present solution scheme has been confirmed by comparing with various existing solutions. Selected numerical results are presented to demonstrate the influence of various parameters such as poroelastic material parameters, embedded depth, foundation aspect ratio etc., on the compliances of a rectangular plate.

1.2 Objectives of Present Study

The main objectives of the present study are given as follows :

1. To develop an efficient numerial scheme to investigate the dynamic interaction between a rigid plate and a multi-layered poroelastic medium
2. To investigate the influence of various parameters such as poroelastic material properties, frequency of excitation, embedded depths, length to width ratio of the plate on the compliances of rigid rectangular plate.

1.3 Basic Assumptions

This study is based on the following assumptions.

1. Each layer of a multi-layered poroelastic medium is homogenous, and governed by Biot's poroelastodynamics theory. All layer interfaces are assumed to be perfectly bonded, i.e. no separation occurs.
2. The plate under consideration is assumed to be massless and rigid.
3. The contact surface between a rigid plate and a poroelastic medium is assumed to be fully bonded and permeable.

Chapter 2
Literature Reviews

In the past, majority of previous researches considered the dynamic interaction between a rectangular plate and a supporting soil medium by modeling the soil domain as a single-phased elastic material. For example, Thomson and Kobori (1963) determined the ground compliance of rectangular slab subjected to the horizontal shear and rocking motions. Luco and Westmann (1972) studied the case of a rectangular strip bonded to the homogenous elastic medium. The coupled rocking and sliding responses of a rectangular plate is considered by Urlich and Kuhlemeyer (1973), by employing the finite element method with the energy absorbing boundary. Wong and Luco (1976) presented the harmonic response of rectangular foundation on elastic half-space by considering the vertical, rocking and horizontal motions. Luco and Wong (1977) and Rüucker (1982) considered vibrations of rectangular foundations bonded to an elastic medium subjected to the horizontal excitation wave. Triantafyllidis (1986) studied the dynamic response of rigid rectangular foundation perfectly bonded to the soil medium by using the Bubnov-Galerkin method, in which the soil medium is modeled as a homogenous isotropic elastic half-space. The three dimensional response between a flexible plate and an elastic half-space was also investigated by Whittaker and Christiano (1982). Recently, the coupled finite element-boundary element (FE-BE) was employed to solve the dynamic response of rectangular raft foundations on an elastic half-space by Mandal and Roychowdhury (2008). In addition, Amiri-Hezaveh et al (2013) investigated dynamic response of a rectangular plate resting on a multi-layered transversely isotropic elastic medium.

Geomaterials often consists of two phases, i.e. solid and voids filled with water, and commonly known as poroelastic materials, and they are considered to be more suitable to represent soils and rocks than ideal elastic materials. Biot (1956 a,b) presented the classical theory of propagation of elastic wave in a poroelastic medium by adding the inertia terms to his quasi-static theory (1941). In the case of layered poroelastic media, Rajapakse and Senjuntichai (1995) developed an exact stiffness matrix method to study dynamic response of a multi-layered pororelastic medium under

a plane strain condition. The elements of a layer stiffness matrix are obtained analytically from the general solution of a homogenous poroelastic medium derived earlier by Senjuntichai and Rajapakse (1994). A propagator matrix method was also employed by several researchers to study dynamic response of a multi-layered poroelastic medium (for example, Pan, 1999 and Zheng et al, 2013). In addition, dynamic response of a multi-layered poroelastic half-space under axisymmetric loading was also investigated by using transmission reflection matrix approach (Lu and Hanya, 2005).

The study of dynamic soil-structure interaction involving a poroelastic medium has also been considered by many researchers. Philippacopoulos (1989) studied the dynamic response of interaction between circular rigid disk and saturated multi-layered half-space. Veklich (1992) considered the resulting of the potential flow due to a plate on a half-space by using the virtual mass and virtual moment of inertia coefficient. The interaction problem was formulated by using a finite difference energy method, and the obtained results are compared with testing data. The impedance of rigid strip bonded to a layered medium was presented by Senjuntichai and Rajapakse (1996) under time-harmonic vertical, horizontal and moment loading. The analysis of a rigid disk embedded in a homogeneous poroelastic half-space under axisymmetric vertical loading can be found in the work of Zeng and Rajapakse (1999), who employed the Hankle integral transform and a discretization technique. Dynamic interaction between a flexible circular plate and a multi-layered poroelastic half-space was later considered by Senjuntichai and Sapsathiarn (2003). In the context of a rectangular plate, Halpern and Christiano (1986) presented the vertical and rocking compliances of a rigid rectangular plate on a homogenous poroelastic half-space by using a discretization technique and Green's functions. A review of literature indicates that dynamic interaction between a rectangular plate and a multi-layered poroelastic medium has never reported in the past.

Chapter 3
Theoretical Consideration

3.1 Basic Equation

Consider a poroelastic medium with a Cartesian coordinate system (x, y, z) defined such that the z -axis is a perpendicular to the free surface as shown in Figure 1. Following Biot's theory of a two-phased material (Biot, 1941), the constitutive relations for a homogenous poroelastic material can be written by using the indicial notation as

$$\sigma_{ij} = 2\mu\varepsilon_{ij} + \lambda\delta_{ij}e - \alpha\delta_{ij}p \quad , \qquad i, j = x, y, z \tag{3.1}$$

$$p = -\alpha Me + M\zeta \tag{3.2}$$

In addition the above equations, σ_{ij} is the total stress component of the bulk material; ε_{ij} and e are the strain component and the dilatation of the solid matrix respectively; p is the excess pore fluid pressure (suction is considered negative); ζ is the variation of fluid content per unit reference volume; δ_{ij} is the Kronecker delta; μ and λ are Lame'constants of the bulk material. In addition, α and M are Biot's parameters accounting for compressibility of a two-phased material. It is written that $0 \le \alpha \le 1$ and $0 \le M \le \infty$ for all poroelastic materials. For a completely dry material, $\alpha = 0$ and $M = 0$.

Let $u_i(x, y, z)$ and $w_i(x, y, z)$ be the average displacement of the solid matrix and the fluid displacement relative to the solid matrix, in the $i-$direction (x, y, z), respectively. The equations of motion of a poroelastic material in the absence of body force (solid and fluid) and a fluid source can be written in terms of displacements u_i and w_i as (Biot, 1962)

$$\mu u_{i,jj} + (\lambda + \alpha^2 M + \mu)u_{i,ji} + \alpha M w_{j,ji} = \rho\ddot{u}_i + \rho_f\ddot{w}_i \tag{3.3}$$

$$\alpha M u_{j,ji} + M w_{j,ji} = \rho_f\ddot{u}_i + m\ddot{w}_i + b\dot{w}_i \tag{3.4}$$

where the superscript dot is used to represent the derivative with respect to the time parameter (t); ρ and ρ_f are the mass densities of the bulk material and the pore fluid

respectively; m is a density-like parameter that depends on ρ_f and the geometry of the pores. In addition, b is parameter accounting for the internal friction due to the relative motion between the solid matrix and the pore fluid. If the internal friction is neglected, then $b=0$.

The motion under consideration is assumed to be time-harmonic with the factor of $e^{i\omega t}$,where ω is the frequency of the excitation and $i=\sqrt{-1}$ .The term $e^{i\omega t}$ is henceforth omitted from all expressions for brevity.

The double Fourier integral transform of a function $f(x,y,z)$ with respect to the horizontal coordinates *x* and *y* can be expressed as (Sneddon, 1951)

$$\bar{f}(k_x,k_y,z)=\int_{-\infty}^{\infty}\int_{-\infty}^{\infty} f(x,y,z)e^{-ik_x x-ik_y y}dxdy \tag{3.5}$$

and the inverse relationship is given by

$$f(x,y,z)=\frac{1}{(2\pi)^2}\int_{-\infty}^{\infty}\int_{-\infty}^{\infty} \bar{f}(k_x,k_y,z)e^{ik_x x+ik_y y}dk_x dk_y \tag{3.6}$$

In addition, the symbol $^-$ denotes the triple-dimensional Fourier transform.

The equation of motions, equations (3.3) and (3.4), can be solved by using a Helmholtz representation for a displacement vector and applying the double Fourier integral transform, given by equation (3.5). The general solutions for the solid and fluid displacements, pore pressure and stresses can be expressed as,

$$\bar{p}=Ae^{-\gamma_1 z}+Be^{\gamma_1 z}+Ce^{-\gamma_2 z}+De^{\gamma_2 z} \tag{3.7}$$

$$\begin{aligned}\bar{u}_x=&-\mathrm{i}k_x\left(a_1Ae^{-\gamma_1 z}+a_1Be^{\gamma_1 z}+a_2Ce^{-\gamma_2 z}+a_2De^{\gamma_2 z}\right)-\frac{\mathrm{i}\gamma_3}{k_x}\left(Ee^{-\gamma_3 z}-Fe^{\gamma_3 z}\right)\\&-\frac{\mathrm{i}k_y}{k_x}\left(Ge^{-\gamma_3 z}+He^{\gamma_3 z}\right)\end{aligned} \tag{3.8}$$

$$\bar{u}_y=-\mathrm{i}k_y\left(a_1Ae^{-\gamma_1 z}+a_1Be^{\gamma_1 z}+a_2Ce^{-\gamma_2 z}+a_2De^{\gamma_2 z}\right)+\mathrm{i}Ge^{-\gamma_3 z}+\mathrm{i}He^{\gamma_3 z} \tag{3.9}$$

$$\bar{u}_z=a_1\gamma_1\left(Ae^{-\gamma_1 z}-Be^{\gamma_1 z}\right)+a_2\gamma_2\left(Ce^{-\gamma_2 z}-De^{\gamma_2 z}\right)+Ee^{-\gamma_3 z}+Fe^{\gamma_3 z} \tag{3.10}$$

$$\bar{w}_z=-h_1\left(Ae^{-\gamma_1 z}-Be^{\gamma_1 z}\right)-h_2\left(Ce^{-\gamma_2 z}-De^{\gamma_2 z}\right)-\vartheta\left(Ee^{-\gamma_3 z}+Fe^{\gamma_3 z}\right) \tag{3.11}$$

$$\bar{\sigma}_{xz} = \mu g_1 \mathrm{i}k_x \left(Ae^{-\gamma_1 z} - Be^{\gamma_1 z}\right) + \mu g_2 \mathrm{i}k_x \left(Ce^{-\gamma_2 z} - De^{\gamma_2 z}\right) + \frac{\mathrm{i}\mu\left(k_x^2 + \gamma_3^2\right)}{k_x}\left(Ee^{-\gamma_3 z} + Fe^{\gamma_3 z}\right) + \frac{\mathrm{i}k_y \mu \gamma_3}{k_x}\left(Ge^{-\gamma_3 z} - He^{\gamma_3 z}\right) \quad (3.12)$$

$$\bar{\sigma}_{yz} = \mu g_1 \mathrm{i}k_y \left(Ae^{-\gamma_1 z} - Be^{\gamma_1 z}\right) + \mu g_2 \mathrm{i}k_y \left(Ce^{-\gamma_2 z} - De^{\gamma_2 z}\right) + \mathrm{i}k_y \mu \left(Ee^{-\gamma_3 z} + Fe^{\gamma_3 z}\right) - \mathrm{i}\gamma_3 \mu \left(Ge^{-\gamma_3 z} - He^{\gamma_3 z}\right) \quad (3.13)$$

$$\bar{\sigma}_{zz} = g_3 \left(Ae^{-\gamma_1 z} + Be^{\gamma_1 z}\right) + g_4 \left(Ce^{-\gamma_2 z} + De^{\gamma_2 z}\right) - 2\mu\gamma_3 \left(Ee^{-\gamma_3 z} - Fe^{\gamma_3 z}\right) \quad (3.14)$$

where

$$\gamma_i^2 = k_x^2 + k_y^2 + L_i^2 \qquad , i = 1, 2 \quad (3.15)$$

$$L_1^2 = \frac{\beta_1 + \sqrt{\beta_1^2 - 4\beta_2}}{2} \quad (3.16)$$

$$L_2^2 = \frac{\beta_1 - \sqrt{\beta_1^2 - 4\beta_2}}{2} \quad (3.17)$$

$$\chi i = \frac{\vartheta M L_i^2 - \rho_f \omega^2}{\rho_f M \omega^2 (\alpha - \vartheta)} \qquad , i = 1, 2 \quad (3.18)$$

$$\beta_1 = \frac{(m\omega^2 - \mathrm{i}b\omega)(\lambda + \alpha^2 M + 2\mu) + \rho M \omega^2 - 2\alpha M \rho_f \omega^2}{M(\lambda + 2\mu)} \quad (3.19)$$

$$\beta_2 = \frac{(m\omega^2 - \mathrm{i}b\omega)\rho\omega^2 - \rho_f^2 \omega^4}{M(\lambda + 2\mu)} \quad (3.20)$$

$$\gamma_3^2 = k_x^2 + k_y^2 - S^2 \quad (3.21)$$

$$S^2 = \frac{k_t^2 \left(\rho - \rho_f \vartheta\right)}{\mu} \quad (3.22)$$

$$a_i = \frac{\lambda\chi_i + \mu\chi_i - \alpha + \vartheta}{\mu\left(S^2 - L_i^2\right)} \qquad , i = 1, 2 \quad (3.23)$$

$$h_i = \left(\frac{1}{\rho_f k_t^2} + a_i\right)\gamma_i \vartheta \qquad , i = 1, 2 \quad (3.24)$$

$$g_i = 2a_i\gamma_i \qquad , i = 1, 2 \quad (3.25)$$

$$g_3 = \lambda\chi_1 - 2\mu a_1 \gamma_1^2 - \alpha \quad (3.26)$$

$$g_4 = \lambda\chi_2 - 2\mu a_2\gamma_2^2 - \alpha \tag{3.27}$$

In addition, $A(\mathrm{k}_x, k_y)$, $B(\mathrm{k}_x, k_y)$, …. , $H(\mathrm{k}_x, k_y)$ are the arbitrary functions to be established by using appropriate boundary and continuity conditions.

3.2 Influence Functions

An exact stiffness matrix describing the relationship between generalized displacement and force vectors of a finite layer and a half-space are derived explicitly in the Fourier transform space. The global stiffness matrix of a layered system is assembled by considering the continuity of traction and fluid flow at each layer interface. In this section, the method is extended from the technique successfully employed to investigate the dynamic response of a multi-layered poroelastic half-plane (Rajapakse and Senjuntichai, 1995).

The general solutions in equation (3.7) - (3.14) can be expressed in the Fourier-transform domain in the following matrix form as

$$\mathbf{v}(k_x, k_y, z) = \mathbf{R}(k_x, k_y, z)\mathbf{c}(k_x, k_y) \tag{3.28}$$

$$\mathbf{f}(k_x, k_y, z) = \mathbf{S}(k_x, k_y, z)\mathbf{c}(k_x, k_y) \tag{3.29}$$

where

$$\mathbf{v}(k_x, k_y, z) = \left[\mathrm{i}\bar{u}_x \ \mathrm{i}\bar{u}_y \ \bar{u}_z \ \bar{p}\right]^T \tag{3.30}$$

$$\mathbf{f}(k_x, k_y, z) = \left[\mathrm{i}\bar{\sigma}_{xz} \ \mathrm{i}\bar{\sigma}_{yz} \ \bar{\sigma}_{zz} \ \bar{w}_z\right]^T \tag{3.31}$$

$$\mathbf{c}(k_x, k_y) = \left[A \ B \ C \ D \ E \ F \ G \ H\right]^T \tag{3.32}$$

$$\mathbf{R}(k_x, k_y, z) = \left[\mathbf{R}_1(k_x, k_y, z) \ \vdots \ \mathbf{R}_2(k_x, k_y, z)\right] \tag{3.33}$$

$$\mathbf{S}(k_x, k_y, z) = \left[\mathbf{S}_1(k_x, k_y, z) \ \vdots \ \mathbf{S}_2(k_x, k_y, z)\right] \tag{3.34}$$

In addition, the superscript T indicates the transpose of a vector or matrix. The arbitrary functions $A_i(k_x, k_y)$ to $H_i(k_x, k_y)$ appearing in $\mathbf{c}(k_x, k_y)$ can be obtained by employing appropriate boundary and continuity conditions. The matrices $\mathbf{R}_i(k_x, k_y, z)$ and $\mathbf{S}_i(k_x, k_y, z)$, where $i = 1, 2$, are given by

$$\mathbf{R}_1(k_x,k_y,z,\omega)=\begin{bmatrix} a_1k_xe^{-\gamma_1 z} & a_1k_xe^{\gamma_1 z} & a_2k_xe^{-\gamma_2 z} & a_2k_xe^{\gamma_2 z} \\ a_1k_ye^{-\gamma_1 z} & a_1k_ye^{\gamma_1 z} & a_2k_ye^{-\gamma_2 z} & a_2k_ye^{\gamma_2 z} \\ a_1r_1e^{-\gamma_1 z} & -a_1r_1e^{\gamma_1 z} & a_2r_2e^{-\gamma_2 z} & -a_2r_2e^{\gamma_2 z} \\ e^{-\gamma_1 z} & e^{\gamma_1 z} & e^{-\gamma_2 z} & e^{\gamma_2 z} \end{bmatrix} \tag{3.35}$$

$$\mathbf{R}_2(k_x,k_y,z,\omega)=\begin{bmatrix} \frac{r_3}{k_x}e^{-\gamma_3 z} & -\frac{r_3}{k_x}e^{\gamma_3 z} & \frac{k_y}{k_x}e^{-\gamma_3 z} & \frac{k_y}{k_x}e^{\gamma_3 z} \\ 0 & 0 & -e^{-\gamma_3 z} & -e^{\gamma_3 z} \\ e^{-\gamma_3 z} & e^{\gamma_3 z} & 0 & 0 \\ 0 & 0 & 0 & 0 \end{bmatrix} \tag{3.36}$$

$$\mathbf{S}_1(k_x,k_y,z,\omega)=\begin{bmatrix} -\mu g_1k_xe^{-\gamma_1 z} & \mu g_1k_xe^{\gamma_1 z} & -\mu g_2k_xe^{-\gamma_2 z} & \mu g_2k_xe^{\gamma_2 z} \\ -\mu g_1k_ye^{-\gamma_1 z} & \mu g_1k_ye^{\gamma_1 z} & -\mu g_2k_ye^{-\gamma_2 z} & \mu g_2k_ye^{\gamma_2 z} \\ g_3e^{-\gamma_1 z} & g_3e^{\gamma_1 z} & g_4e^{-\gamma_2 z} & g_4e^{\gamma_2 z} \\ -h_1e^{-\gamma_1 z} & h_1e^{\gamma_1 z} & -h_2e^{-\gamma_2 z} & h_2e^{\gamma_2 z} \end{bmatrix} \tag{3.37}$$

$$\mathbf{S}_2(k_x,k_y,z,\omega)=\begin{bmatrix} -\frac{\mu\left(k_x^2+\gamma_3^2\right)}{k_x}e^{-\gamma_3 z} & -\frac{\mu\left(k_x^2+\gamma_3^2\right)}{k_x}e^{\gamma_3 z} & -\frac{\mu k_y\gamma_3}{k_x}e^{-\gamma_3 z} & \frac{\mu k_y\gamma_3}{k_x}e^{\gamma_3 z} \\ -\mu k_ye^{-\gamma_3 z} & -\mu k_ye^{\gamma_3 z} & \mu\gamma_3e^{-\gamma_3 z} & -\mu\gamma_3e^{\gamma_3 z} \\ -2\mu\gamma_3e^{-\gamma_3 z} & 2\mu\gamma_3e^{\gamma_3 z} & 0 & 0 \\ -\vartheta e^{-\gamma_3 z} & -\vartheta e^{\gamma_3 z} & 0 & 0 \end{bmatrix} \tag{3.38}$$

Consider a multi-layered poroelastic medium consisting of *N* poroelastic layers overlying a poroelastic half-space as shown in Figure 1.The stress and displacement relationship at the top and the bottom surfaces of an *n* layer (*n*=1,2,3..,*N*) can be obtained as

$$\mathbf{u}^{(n)}=\begin{bmatrix} \mathbf{R}^{(n)}(k_x,k_y,z_n) \\ \cdots\cdots\cdots\cdots \\ \mathbf{R}^{(n)}(k_x,k_y,z_{(n+1)}) \end{bmatrix}\mathbf{c}^{(n)} \tag{3.39}$$

$$\boldsymbol{\sigma}^{(n)}=\begin{bmatrix} -\mathbf{S}^{(n)}(k_x,k_y,z_n) \\ \cdots\cdots\cdots\cdots \\ \mathbf{S}^{(n)}(k_x,k_y,z_{(n+1)}) \end{bmatrix}\mathbf{c}^{(n)} \tag{3.40}$$

where

$$\mathbf{u}^{(n)} = \left[\begin{array}{cc} \mathbf{v}^{(n)}(k_x, k_y, z_n) & \mathbf{v}^{(n)}(k_x, k_y, z_{n+1}) \end{array} \right]^T \tag{3.41}$$

$$\boldsymbol{\sigma}^{(n)} = \left[\begin{array}{cc} -\mathbf{f}^{(n)}(k_x, k_y, z_n) & \mathbf{f}^{(n)}(k_x, k_y, z_{n+1}) \end{array} \right]^T \tag{3.42}$$

In the above equation, $\mathbf{u}^{(n)}$ denotes a column vector of generalized displacements for the nth layer whose elements are the Fourier transforms of displacements and pore pressure at the top and bottom surfaces of the nth layer. Similarly, $\boldsymbol{\sigma}^{(n)}$ denotes a column vector of generalized forces whose elements are the Fourier transforms of traction and fluid displacements of the top and bottom surfaces of the nth layer.

The matrices $\mathbf{R}^{(n)}$ and $\mathbf{S}^{(n)}$ are identical to $\mathbf{R}$ and $\mathbf{S}$ defined in equation (3.33) to (3.38) except that the material properties of the nth layer being used in the definition and $z = z_n$ or z_{n+1}. The vector $\mathbf{c}^{(n)}$ is the arbitrary coefficient vector corresponding to the nth layer.

The equation (3.39) can be inverted to express $\mathbf{c}^{(n)}$ in terms of $\mathbf{u}^{(n)}$, and the substitution into equation (3.40) results in the following matrix equation.

$$\boldsymbol{\sigma}^{(n)} = \mathbf{K}^{(n)}\mathbf{u}^{(n)} \tag{3.43}$$

where $\mathbf{K}^{(n)}$ is an exact stiffness matrix in the Fourier transform space describing the relationship between the generalized displacement vector $\mathbf{u}^{(n)}$ and the force vector $\boldsymbol{\sigma}^{(n)}$ for the nth layer.The explicit expressions of all elements in $\mathbf{K}^{(n)}$ are given elsewhere (Yooyao, 2008).

For the underlying half-space, the following relationship can be established,

$$\boldsymbol{\sigma}^{(N+1)} = \mathbf{K}^{(N+1)}\mathbf{u}^{(N+1)} \tag{3.44}$$

where

$$\mathbf{u}^{(N+1)} = \left[\begin{array}{c} \mathbf{v}^{(N+1)}(k_x, k_y, z_{N+1}) \end{array} \right]^T \tag{3.45}$$

$$\boldsymbol{\sigma}^{(N+1)} = \left[-\mathbf{f}^{(N+1)}(k_x, k_y, z_{N+1}) \right]^T \tag{3.46}$$

$$\mathbf{K}^{(N+1)} = symm.[\tilde{k}_{ij}]_{4x4} \tag{3.47}$$

It is noted that exponential terms of k_x and k_y are not involved in the expression of $\mathbf{K}^{(n+1)}$, and its elements depend on the material properties of the underlying half-space and the Fourier transform parameters k_x and k_y. The elements of the stiffness matrix $\mathbf{K}^{(n+1)}$ were also given explicitly by Yooyao (2008).

The global stiffness matrix of a multi-layered half-space is assembled by using the layer and half-space stiffness matrices together with the continuity conditions of traction and fluid flow at the layer interfaces. For instance, the continuity conditions at the nth interface can be written as

$$\mathbf{f}^{(n-1)}(k_x, k_y, z) - \mathbf{f}^{(n)}(k_x, k_y, z) = \mathbf{t}^{(n)} \tag{3.48}$$

where $\mathbf{f}^{(n)}$ is identical to $\mathbf{f}$ in equation (3.31) with a superscript n denoting the layer number and

$$\mathbf{t}^{(n)} = \left[\bar{T}_x^{(n)} \;\; \bar{T}_y^{(n)} \;\; \bar{T}_z^{(n)} \;\; \frac{\bar{Q}_z^{(n)}}{i\omega} \right]^T \tag{3.49}$$

In equation (3.49), $\bar{T}_i^{(n)}\,(i = x, y, z)$ is the Fourier transform of the loading in the $i-$direction $(i = x, y, z)$ applied at the nth interface. In addition, $\bar{Q}_z^{(n)}$ is the Fourier transform of the fluid source applied at the nth interface. If the nth interface is not subjected to any external loading or fluid source then $\mathbf{t}^{(n)}$ is a null vector.

The consideration of equation (3.48) at each layer interface together with equations (3.43) and (3.44) result in the following global equation system.

$$\begin{bmatrix} \mathrm{K}^{(1)} & & & \\ & \mathrm{K}^{(2)} & & \\ & & \ddots & \\ & & & \mathrm{K}^{(N)} \;\; \mathrm{K}^{(N+1)} \end{bmatrix} \begin{Bmatrix} \mathrm{u}^{(1)} \\ \mathrm{u}^{(2)} \\ \vdots \\ \mathrm{u}^{(N)} \\ \mathrm{u}^{(N+1)} \end{Bmatrix} = \begin{Bmatrix} \mathrm{t}^{(1)} \\ \mathrm{t}^{(2)} \\ \vdots \\ \mathrm{t}^{(N)} \\ \mathrm{t}^{(N+1)} \end{Bmatrix} \tag{3.50}$$

The global stiffness matrix shown in equation (3.50) is a well-conditioned symmetric matrix with a size equal to eight. The number of unknowns in the final global equation system is equal to $4(N+1)$. The solution of the equation (3.50) yields the

Fourier transforms of the influence functions for analysis of interaction between a rigid plate and a multi-layered poroelastic medium.

The influence functions, expressed in term of a semi-infinite integral, can be obtained by using the discretization technique [see Figure 2 (b)]. First, the contact surface under the plate is divided into a finite number of small rectangular areas. Nodal points are selected at the center of each discretized region. Each region is then subjected to uniform traction of unit intensity applied at the $i-$ direction $(i = x, y, z)$. The influence functions, which are required to establish the flexibility equation system for analysis of this interaction problem, are obtained from the displacements computed at each nodal point of discretized regions. The applied traction over a sub-region with the size of $2l \times 2w$ and its nodal point located at a point (x_i, y_j) can be expressed as [see Figure 2 (b)],

$$T(x_i, y_j) = [H(x_i + l) - H(x_i - l)][H(y_j + w) - H(y_j - w)] \tag{3.51}$$

By applying the Fourier transform, equation (3.5), to the above equation,

$$\bar{T}(k_x, k_y) = \frac{4\sin(k_x l)\sin(k_y w)}{k_x k_y} \tag{3.52}$$

where H denotes the Heaviside function.

3.3 Formulation of Interaction Problem

Consider a rigid rectangular plate of size $2a \times 2A$ bonded to a multi-layered poroelastic half-space illustrated in Figure 1. The plate is subjected to time-harmonic vertical, horizontal and rocking loading, respectively as shown in Figure 2 (a). The contact surface between a plate and a multi-layered medium is assumed to be fully permeable and the surface traction between the plate and the supporting medium is unknown. The displacements of the rigid plate can be expressed in terms of three translation components and three rotation components as,

$$u_x = \Delta_x - \theta_z y \tag{3.53}$$

$$u_y = \Delta_y + \theta_z x \tag{3.54}$$

$$u_z = \Delta_z + y\theta_x - x\theta_y \tag{3.55}$$

on $|x| \le a, |y| \le A$. In addition, $\Delta_i (i = x, y, z)$ corresponds to the displacement amplitudes at the center of area, $\theta_i (i = x, y, z)$ corresponds to the amplitudes of the rotation about the x, y and z-axes, respectively. These equations can be expressed in the matrix form as

$$\boldsymbol{U} = \Omega \Delta \tag{3.56}$$

where $\boldsymbol{U} = \{u_x, u_y, u_z\}^{\mathrm{T}}$, $\Delta = \{\Delta_x, \Delta_y, \Delta_z, \theta_x, \theta_y, \theta_z\}^{\mathrm{T}}$ and Ω is a 3×6 matrix, which can be expressed as,

$$\Omega = \begin{bmatrix} 1 & 0 & 0 & 0 & 0 & -y \\ 0 & 1 & 0 & 0 & 0 & x \\ 0 & 0 & 1 & y & -x & 0 \end{bmatrix} \tag{3.57}$$

The contact traction between the foundation and the supporting medium can be expressed in terms of the translations and the rotations of the rigid plate. The contact traction in the $i-$direction $(i = x, y, z)$ at the contact interface between the plate and the supporting medium due to the applied loading are denoted by T_x, T_y and T_z respectively. The equations of equilibrium of forces applied to the rigid plate shown in Figure 2 (a) can then be expressed as,

$$F_i = -\int_A T_i dA \quad (i = x, y, z) \tag{3.58}$$

$$M_x = -\int_A T_z y dA \tag{3.59}$$

$$M_y = -\int_A T_z x dA \tag{3.60}$$

$$M_z = -\int_A [T_y x - T_x \, \mathrm{y}] dA \tag{3.61}$$

Consequently, the following relationship can be established

$$\boldsymbol{F} = \Omega^{\mathrm{T}} \boldsymbol{T} \tag{3.62}$$

where $\boldsymbol{F} = \{F_x, F_y, F_z, M_x, M_y, M_z\}^{\mathrm{T}}$ and $\boldsymbol{T} = \{T_x, T_y, T_z\}^{\mathrm{T}}$. In addition, the matrix Ω is given by equation (3.57).

By using the discretizing technique outlined in the previous chapter, the influence Green's functions, for determining the unknown traction, can be represented as

$$\boldsymbol{G}\,\boldsymbol{T} = \boldsymbol{U} \tag{3.63}$$

where

$$G_{ij} = \begin{bmatrix} G_{xx} & G_{xy} & G_{xz} \\ G_{yx} & G_{yy} & G_{yz} \\ G_{zx} & G_{zy} & G_{zz} \end{bmatrix} \tag{3.64}$$

In view of equations (3.56), (3.62) and (3.63), the following relationship can be established

$$\boldsymbol{F} = \boldsymbol{K}\ \Delta \tag{3.65}$$

where $\boldsymbol{K}$ is a non-dimensional impedance matrix defined as

$$\boldsymbol{K} = \mu a \begin{bmatrix} K_{hh} & 0 & 0 & 0 & K_{hm} & 0 \\ 0 & K_{hh} & 0 & -K_{hm} & 0 & 0 \\ 0 & 0 & K_{vv} & 0 & 0 & 0 \\ 0 & -K_{mh} & 0 & K_{mm} & 0 & 0 \\ K_{mh} & 0 & 0 & 0 & K_{mm} & 0 \\ 0 & 0 & 0 & 0 & 0 & K_{tt} \end{bmatrix} \tag{3.66}$$

Finally, the response of rigid rectangular plate is characterized by the following non-dimensional compliance matrix,

$$\Delta = \boldsymbol{C}\boldsymbol{F} \tag{3.67}$$

where

$$\boldsymbol{C} = \frac{1}{\mu a} \begin{bmatrix} C_{hh} & 0 & 0 & 0 & C_{hm} & 0 \\ 0 & C_{hh} & 0 & -C_{hm} & 0 & 0 \\ 0 & 0 & C_{vv} & 0 & 0 & 0 \\ 0 & -C_{mh} & 0 & C_{mm} & 0 & 0 \\ C_{mh} & 0 & 0 & 0 & C_{mm} & 0 \\ 0 & 0 & 0 & 0 & 0 & C_{tt} \end{bmatrix} \tag{3.68}$$

The matrix $\boldsymbol{C}$ shown in the above equation is a 6×6 symmetric complex frequency-dependent compliance matrix. The methodology outlined in this chapter does not discuss an issue regarding the singularities of the contact traction along the

edge of the plate. Nevertheless, the evaluation of the compliance matrix should be accurate enough for practical applications.

Chapter 4
Numerical Solution

This chapter is concerned with the numerical results obtained from the solution scheme described in chapter 3. A computer program has been developed to investigate the dynamic interaction between a rigid rectangular plate and a multi-layered poroelastic medium. Both homogenous and multi-layered poroelastic media are considered. In addition, the vertical, horizontal, rocking, coupling and torsion compliances are determined by employing the numerical solution scheme outlined in the previous chapter. The convergence is discussed and the accuracy of the present solution scheme is verified by comparing with existing solutions. Numerical results are presented in this chapter to demonstrate the applicability of the present solution scheme and to portray the influence of various parameters on the compliances of the rectangular plate.

4.1 Numerical Solution Schemce

A computer program has been developed based on the procedure described previously to investigate the dynamic interaction problem between rigid rectangular plate and multi-layered poroelastic media. The tasks performed by the computer code can be summarized as:

1. The contact area under the rectangular plate is divided into $N_x \times N_y$ square discretized regions as shown in Figure 2 (b).
2. The influence functions are determined to establish the equation (3.63) for the determination of the unknown contact traction.
3. The corresponding vertical, horizontal, rocking, coupling and torsion compliances of the rectangular plate are obtained.

4.2 Numerical Results and Discussion

4.2.1 Convergence of present solution.

The convergence and accuracy of the numerical solution scheme are first investigated with respect to the number of elements, $N_x \times N_y$, used to discretize the

contact area [see Figure 3 (a)]. Figure 4 presents the convergence and accuracy of non-dimensional vertical compliance of a rigid rectangular plate resting on the surface of a homogenous elastic half-space (Poisson ratio=0.333) by Wong and Luco (1976) , for different values of $N_x \times N_y$. It appears from Figure 4 (a) that converged and accurate numerical results are obtained when $N_x \times N_y \geq 8 \times 8$.

Figure 4 (b) shows the convergence and accuracy of non-dimensional vertical compliance of a rigid circular disk resting on the surface of a homogenous poroelastic half-space. All length parameters in the numerical study are non-dimensionalized with respect to a half-width of rectangular plate, *a*, i.e., $x^* = x/a$, $y^* = y/a$, $z^* = z/a$. The normalized frequency is defined as $\delta = \omega a\sqrt{\rho/\mu}$. In addition, the non-dimensional material properties are defined as $\lambda^* = \lambda/\mu$, $M^* = M/\mu$, $\rho_f^* = \rho_f/\rho$, $m^* = m/\rho$ and $b^* = ab/\sqrt{\rho\mu}$. Note that the shear modulus and the mass density of the top layer, denoted by $\mu^{(1)}$ and $\rho^{(1)}$, respectively, are employed in the normalization in the numerical results involving a multi-layered medium.

The properties of poroelastic materials considered in Figure 4 (b) are as follows: $b^* = 2.3$, $\lambda^* = 1.0$, $M^* = 12.2$, $\rho^*_f = 0.53, \alpha = 0.97$ and $m^* = 1.1$. It appears from the Figure 4 (b) that converged and accurate numerical results are obtained when $N_x \times N_y \geq 8 \times 8$. Note that the total number of elements in this case are reduced from 64 elements to 52 elements to simulate the geometry of a circular disk as shown in the Figure 3 (b).

4.2.2 Comparison with existing solutions

The accuracy of the present solution scheme of interaction problem is validated by comparing the numerical results obtained from the present scheme with various existing solutions.

Figure 5 presents the comparison of numerical solutions corresponding to the profiles of displacements along the *z* -axis in a homogenous poroelastic half-space between the present solutions and the solutions given by Zheng et al (2013). The material properties of the poroelastic medium are $b^* = 1.0$ $\lambda^* = 1.0$, $M^* = 2.0$,

$\rho_f^* = 0.5$, $\alpha = 0.90$ and $m^* = 2.0$. Both vertical and horizontal displacements under the vertical and horizontal loads applied at the level $z^* = 1$ are presented. It is evident from Figure 5 that very good agreement between the two solutions is obtained.

Figure 6 (a) presents the comparison of the compliances of rigid rectangular plate resting on a homogenous elastic half-space with the Poisson's ratio of 0.333 given by Wong and Luco (1978) . The vertical, horizontal, rocking and coupling motions are investigated. Figure 6 (b) presents the vertical compliances of a circular disk with fully permeable contact surface buried in different depths in a homogenous poroelastic half-space considered by Zeng and Rajapakse (1999). The properties of poroelastic materials are $b^* = 2.3$, $\lambda^* = 1.0$, $M^* = 12.2$, $\rho_f^* = 0.53$, $\alpha = 0.97$ and $m^* = 1.1$.

The non-dimensional vertical compliance of a rigid disk is defined by $C_{vv} = \left(\Delta_z / \mathrm{F}_z\right) / C_{vv}^*$ in which Δ_z is the vertical displacement of a rigid disk , F_z is the magnitude of vertical loading and C_{vv}^* is the vertical compliance of a circular disk embedded in an ideal elastic half-space under static loading. Note that $C_{vv}^* = \left(1-\nu\right) / 4\mu a$. The accuracy of the present solution scheme is once again confirmed through the comparisons shown in Figure 6.

Figure 7 presents the traction profile of a circular disk resting on a homogenous poroelastic half-space by Senjuntichai and Sapsathiarn (2003). The surface traction is defined by $T_z^* = T_z \pi a / F_z$. The contact traction profiles are presented along the radius of the disk. The number of elements $\left(N_x \times N_y\right)$ equal to 9×9 and 17×17, and the frequencies of $\delta =$ 0.5 and 3.0 are considered. It can be seen the Figure 7 that shows good agreement between the two solutions are obtained when $N_x \times N_y \geq 17\times17$.

4.2.3 Dynamic response of a multi-layered poroelastic medium.

The dynamic response of a multi-layered poroelastic medium subjected to the surface loading is considered in this sub-section as shown in Figure 8. The thickness of the top layer is equal to '*a*'. The properties of the top layer are different for five systems as shown in Figure 9, and there are identified in Table 1. The properties of the underlying half-space are identical to those of 'MB'. The rectangular vertical and horizontal loading of uniform intensities p_0 and q_0 respectively applied over a square

area of 2×2 at the top surface are considered. In addition, the numerical solutions at the frequencies of $\delta =$ 0.5 and 3.0 are evaluated.

Figure 10 shows the variations of non-dimensional vertical displacement $u_{zz}^{*} = a\mu^{(1)} u_{zz} / p_0$ along the top surface of the multi-layered half-space under the surface vertical loading. The parameter b represents the internal friction between the solid matrix and the pore fluid. It can be observed that when the parameter b increases, the magnitude of vertical displacement decreases as shown in the real part of the displacement. From $x^{*} =$ 0 to 2 the vertical displacement changes rapidly. In addition, the magnitude of vertical displacement at low frequency is larger than that at high frequency, in which the displacement profiles show oscillatory variations with the horizontal axis.

Figure 11 shows the variations of non-dimensional vertical displacement $u_{zx}^{*} = a\mu^{(1)} u_{zx} / q_0$ along the top surface under the square horizontal loading. Naturally, the magnitude of the vertical displacement due to the horizontal loading is less than that under the vertical loading. The magnitude of vertical displacement is equal to zero at the center of loading, and reaches its maximum value at $x^{*} =$ 1.0, Thereafter, it decreases rapidly when x^{*} is located further away from the center of loading. The magnitude of vertical displacement at low frequency is larger than that at high frequency similar to what observed in the case of vertical loading. In addition, the displacement profiles, once again, show oscillatory variations with the horizontal axis at higher frequency.

4.2.4 Dynamic interaction between rectangular plate and multi-layered poroelastic media

In this sub-section, the dynamic interaction between a rigid rectangular plate and a multi-layered poroelastic medium is considered. The geometry of problem under consideration is shown in Figure 12. The accuracy of the present solution scheme of this interaction problem is first verified by comparing with existing solutions.

Two kinds of multi-layered poroelastic media are considered, i.e. two-layered and three-layered systems. For a two-layered system, a multi-layered poroelastic half-space consists of one layer and an underlying half-space as shown in Figure 12. There are five cases under consideration for this two-layered system as shown in Figure 9.

The thickness of the first layer is fixed at $h_1 = a$ for all cases, and the material properties for each system are given in Table 1.

For convenience, the modification of the contact condition is considered. The friction beneath the plate is neglected for the vertical loading, whereas, it is taken into account for the horizontal and the rocking motions. The compliances are thus defined as:

$C_{vv} = \mu a \Delta_z / F_z$ for the vertical compliance

$C_{hh} = \mu a \Delta_x / F_x$ for the horizontal compliance in x-direction

$C_{mm} = \mu a^3 \theta_x / M_y$ for the rocking compliance

$C_{hm} = \mu a^3 \Delta_z / M_y$ for the coupling compliance

$C_{tt} = \mu a^3 \theta_z / M_z$ for the torsion compliance

Figure 13 to Figure 16 illustrate the influence of the parameter b on the dynamic interaction between the rectangular plate and the two-layered systems. Figure 13 and Figure 14 show the vertical and horizontal compliances of the rigid plate respectively. Similar behaviors are observed for the vertical and the horizontal compliances. The vertical and horizontal compliances decrease as the frequency increases for all values of b. The parameter b has a significant influence on the compliances since higher compliances are obtained as b decreases. At low frequency, the abrupt decrease of both vertical and horizontal compliances was observed. More significant differences among different layer systems are observed in the vertical compliances than that in the horizontal compliances.

Figure 15 and Figure 16 show the rocking and torsion compliances of a rectangular plate. Similar behaviors are noted for both compliances, and more significant influence are observed on the rocking motion. Both compliances gradually increase with frequency before reaching to the maximum values when $\delta > 1$. The coupling compliances for different two-layered systems are also shown in Figure 17. It can be found that the parameter b shows more significant influence in the case of the coupling compliances when compared to other compliances.

Next, the influence of the plate embedded depth *(h/a)* on the compliances is investigated. In this study, MC is chosen for the top layer and MB for the bottom layer. The embedded depth is varied as h/a = 0, 1, 2, and 5.

Figure 18 and Figure 19 present the vertical compliance and the horizontal compliance of a rigid rectangular plate. It can be observed that when the embedded depth increases, the magnitude of the both compliances are decreased. At low frequency range $(0<\delta<2)$, both compliances decrease rapidly. The variation of vertical and horizontal compliances of a surface plate $(h/a=0)$ is smooth for both real and imaginary parts. As expected, for embedded plates $(h/a=1,2,5)$, both compliances show oscillatory variations with δ in both real and imaginary parts due to the effect of the standing wave generated between the free surface and the embedded plate as also noted by Zeng and Rajapakse (1999) and Senjuntichai and Sapsathiarn (2003).

Figure 20 and Figure 21 present the rocking and the torsion compliances of a rigid plate at different depths of embedment. Figure 22 shows the coupling compliance due to the coupling between the horizontal and rocking motions. The variation of all compliances of a surface plate $(h/a=0)$ with the frequency is smooth for both real and imaginary parts. However, for embedded plates $(h/a=1,2,5)$, both real and imaginary parts show oscillatory variations with frequency.

The vertical compliances of surface plates $(h/\mathrm{a}=0)$ with different geometries, i.e. the ratios of A/a are varied from 0.25 to 4, are presented in Figure 23. For a square plate, i.e. when A/a is equal to 1.0, the number of elements $N_x \times N_y = 8\times 8$ is used. When A/a is equal to 0.25 and 4.0, the number of elements $N_x \times N_y = 2\times 8$ is employed. In addition, $N_x \times N_y = 4\times 8$ is considered for A/a equal to 0.5 and 2.0. The number of elements used in each case is similar to what employed by Luco and Wong (1976). It should be noted that the ratio of A/a is directly related to the plate stiffness as a larger plate can resist higher force than a smaller one. Vertical, horizontal and rocking compliances of rigid plates of various shapes are also presented in the Figure 24 to Figure 26 respectively. Four types of rigid plates are considered, i.e. circular, square, rectangular and triangular shapes. Note that the dimensions of plates are chosen

such that the contact area between the plate and the poroelastic medium is approximately equal to four in all plate types.

Figure 27 presents the vertical compliances of rectangular plate with an internal square hole as shown in Figure 3 (c). The size of the hole is equal to $2d \times 2d$. The ratio d/a is taken into account and is varied from 0.25 to 0.75. It can be seen that the vertical compliance decreases rapidly in the range $0 < \delta < 2$. In addition, the influence of the opening is significant on the vertical compliance when the ratio d/a is greater than 0.25.

Figure 28 presents the traction profile along the center line of a rigid plate resting on a multi-layered poroelastic medium. Various shapes of plates are considered, i.e. square plate, rectangular plates with and without a square hole. The contact area between the plate and the half-space is approximately equal to four in all plate types. The frequencies of $\delta = 0.5$ and 3.0 are considered. The number of elements $(N_x \times N_y)$ employed in the calculation is 17×17. It can be seen from the figure that the traction around the central area of the plate is flat. The traction increases and reaches its maximum value at the edge of the plate. The traction under the rectangular plate with a square hole, however, shows different behaviors due to the presence of an internal hole. Thus, higher values of contact traction in this type of plates are found along both internal and external edges.

The case of three-layered poroelastic systems are considered next. Two poroelastic layers and an underlying poroelastichalf-space as shown in Figure 29 constitute a three-layered system. Two poroelastic layers of this system are identified as system PA, system PB and system PC. The material properties of three-layered system are given in Table 2. In addition, the parameter b for the first and the second layers and underlying half-space of all systems are given in Table 3. For the system PC, which is a dry material, the required parameters are only μ , λ and ρ for each layer.

Figure 30 to Figure 32 present the vertical, horizontal, and rocking compliances of a rigid rectangular plate embedded $(h/a = 1)$ in a three-layered system as shown in Figure 29. In addition, the thicknesses of the first and second layers are set to be equal to a for all cases, and the material properties for each layered system are given in Table 2 and Table 3. It can be observed from Figure 30 to Figure 32 that all compliances show

oscillatory variations with frequency. It is also observed that all compliance components decrease as the parameter b increases.

Figure 33 to Figure 35 present the influence of layer thickness on the compliance. The system PB is used to investigate this effect. The thickness of the first layer (h_1) is set to be $h_1 / a = 1$, whereas the thickness of second layer (h_2) is varied, i.e. $h_2 / a = 1$, 2, 5, 10, 20 and 25. The case of a two-layered system, i.e. one layer overlying on a homogenous half-space, is also shown for comparison. The material properties of the first layer are given in Table 2 and Table 3, whereas the properties of the underlying half-space are obtained from the second layer given in those tables. It can be observed that the vertical and horizontal compliances show more oscillations when $h_2 / a \le 5$. As the thickness of second layer increases, the compliances of a three-layered system approach those of a two-layered system, and both solution are identical when $h_2 / a \ge 25$ for the vertical compliances and $h_2 / a \ge 20$ for the horizontal compliances. For rocking compliances, the influence of layering under the foundation is negligible when thickness of the second layer is at least five times greater than the foundation width.

Chapter 5
Conclusion

The dynamic interaction between a rigid rectangular plate and a multi-layered poroelastic medium is investigated in this thesis. The contact surface between the plate and the supporting medium is assumed to be bonded and fully permeable. The plate is subjected to the time-harmonic vertical, horizontal and moment loading. The cases of rectangular plates resting on the top surface and embedded in a poroelastic stratum both are under consideration in this study. The poroelastodynamic principle given by Biot and the discretization technique are employed. In addition, the exact stiffness matrix scheme is adopted to determine the influence functions required for analysis of this dynamic interaction problem.

The convergence and accuracy of the present solution scheme with respect to $N_x \times N_y$ are first studied. The convergence is found to be stable when $N_x = 8$ and $N_y = 8$ for a square plate. In addition, the accuracy of this present solution is also verified and confirmed by comparing with various existing solutions.

Numerical results presented in Chapter 4 indicate that the interaction between a rigid rectangular plate and a multi-layered poroelastic medium is governed by several parameters. The parameter b shows significant influence on the compliances of the plate since it directly relates to the permeability of a poroelastic medium. The excess pore pressure increases as the value of b increases. The influence of parameter b is more obvious in the cases of vertical and rocking compliances. The frequency of excitation also show significant influence on the plate response. All compliance components show oscillatory variations with higher frequency. In addition, the plate compliances also depend significantly on the embedded depth and the plate aspect ratio. The numerical solution scheme developed in this thesis can be extended to study more practical problems by considering the condition of impermeability at the plate-poroelastic-medium contact surface, and the flexural rigidity of plate.

REFERENCES

Amiri-Hezaveh, A., Eskandari-Ghadi, M., Rahimian, M., and Ghorbani-Tanha, A. K. (2013). Impedance functions for surface rigid rectangular foundations on transversely isotropic multilayer half-spaces. *Journal of Applied Mechanics, 80*(5), 051017.

Biot, M. A. (1941). General theory of three-dimensional consolidation. *Journal of applied physics, 12*(2), 155-164.

Biot, M. A. (1956a). Theory of propagation of elastic waves in a fluid-saturated porous solid. I. Low-frequency range. *The Journal of the acoustical Society of america, 28*(2), 168-178.

Biot, M. A. (1956b). Theory of propagation of elastic waves in a fluid-saturated porous solid. II. Higher frequency range. *The Journal of the acoustical Society of america, 28*(2), 179-191.

Biot, M. A. (1962). Mechanics of deformation and acoustic propagation in porous media. *Journal of applied physics, 33*(4), 1482-1498.

Halpern, M. R., and Christiano, P. (1986). Steady-state harmonic response of a rigid plate bearing on a liquid-saturated poroelastic halfspace. *Earthquake engineering & structural dynamics, 14*(3), 439-454.

Lu, J.-F., and Hanyga, A. (2005). Fundamental solution for a layered porous half space subject to a vertical point force or a point fluid source. *Computational Mechanics, 35*(5), 376-391.

Luco, J., and Westmann, R. (1972). Dynamic response of a rigid footing bonded to an elastic half space. *Journal of Applied Mechanics, 39*(2), 527-534.

Luco, J., and Wong, H. (1977). *Dynamic response of rectangular foundations for Rayleigh wave excitation.* Paper presented at the Proc. 6th World Conf. Earthq. Eng.

Mandal, J., and Roychowdhury, S. (2008). *Response of rectangular raft foundations under transient loading.* Paper presented at the Proceedings, 12th International Conference of International Association for Computer Methods and Advanced in Geomechanis (IACMAG), India.

Pan, E. (1999). Green's functions in layered poroelastic half-spaces. *International Journal for Numerical and Analytical Methods in Geomechanics, 23*(13), 1631-1653.

Philippacopoulos, A. (1989). Axisymmetric vibration of disk resting on saturated layered half-space. *Journal of Engineering Mechanics, 115*(10), 2301-2322.

Rajapakse, R., and Senjuntichai, T. (1995). Dynamic response of a multi-layered poroelastic medium. *Earthquake engineering & structural dynamics, 24*(5), 703-722.

Rüucker, W. (1982). Dynamic behaviour of rigid foundations of arbitrary shape on a halfspace. *Earthquake engineering & structural dynamics, 10*(5), 675-690.

Senjuntichai, T., and Rajapakse, R. (1994). Dynamic Green's functions of homogeneous poroelastic half-plane. *Journal of Engineering Mechanics, 120*(11), 2381-2404.

Senjuntichai, T., and Rajapakse, R. (1996). Dynamics of a rigid strip bonded to a multilayered poroelastic medium *Mechanics of poroelastic media* (pp. 353-369): Springer.

Senjuntichai, T., and Sapsathiarn, Y. (2003). Forced vertical vibration of circular plate in multilayered poroelastic medium. *Journal of Engineering Mechanics, 129*(11), 1330-1341.

Sneddon, I. (1951). *Fourier transform*. McGraw-Hill Book Co: New York.

Thomson, W. T., and Kobori, T. (1963). Dynamical compliance of rectangular foundations on an elastic half-space. *Journal of Applied Mechanics, 30*(4), 579-584.

Triantafyllidis, T. (1986). Dynamic stiffness of rigid rectangular foundations on the half-space. *Earthquake engineering & structural dynamics, 14*(3), 391-411.

Urlich, C., and Kuhlemeyer, R. (1973). Coupled rocking and lateral vibrations of embedded footings. *Canadian Geotechnical Journal, 10*(2), 145-160.

Veklich, N. (1992). Impact of a rectangular plate on a liquid half-space. *Fluid dynamics, 27*(5), 697-702.

Whittaker, W., and Christiano, P. (1982). Response of a plate and elastic half-space to harmonic waves. *Earthquake engineering & structural dynamics, 10*(2), 255-266.

Wong, H., and Luco, J. (1976). Dynamic response of rigid foundations of arbitrary shape. *Earthquake engineering & structural dynamics, 4*(6), 579-587.

Wong, H., and Luco, J. (1978). Dynamic response of rectangular foundations to obliquely incident seismic waves. *Earthquake engineering & structural dynamics, 6*(1), 3-16.

Yooyao, B. (2008). *Dynamic reponse of a multilayered poroelastic medium to moving loads.* (master), Chulalongkorn University, Bangkok, Thailand.

Zeng, X., and Rajapakse, R. (1999). Vertical vibrations of a rigid disk embedded in a poroelastic medium. *International Journal for Numerical and Analytical Methods in Geomechanics, 23*(15), 2075-2095.

Zheng, P., Ding, B., Zhao, S.-X., and Ding, D. (2013). 3D dynamic Green's functions in a multilayered poroelastic half-space. *Applied Mathematical Modelling, 37*(24), 10203-10219.

Table 1 Material properties of a homogenous poroelastic medium

	μ^*	λ^*	M^*	$\rho^\dagger$	$\rho_f^\dagger$	$m^\dagger$	α	b^+
MA	2.0	2.0	24.4	2.0	1.06	2.2	0.97	6.32×10^2
MB	2.0	2.0	24.4	2.0	1.06	2.2	0.97	1.45×10^6
MC	2.0	2.0	24.4	2.0	1.06	2.2	0.97	6.32×10^6
MD	2.0	2.0	24.4	2.0	1.06	2.2	0.97	6.32×10^7
ME	2.0	2.0	-	2.0	-	-	-	-

$^*\times10^8\ N/m^2$ $^\dagger\times10^3\ kg/m^3$ $^+\ N\,s/m^4$

Table 2 Material properties of a three-layered poroelastic medium

	μ^*	λ^*	M^*	$\rho^\dagger$	$\rho_f^\dagger$	$m^\dagger$	α
First layer	2.5	5.0	25.0	2.0	1.0	3.0	0.95
Second layer	1.25	1.88	18.8	1.6	1.0	1.8	0.98
Half-space	10.0	10.0	20.0	2.4	1.0	4.8	0.9

$^*\times10^8\ N/m^2$ $^\dagger\times10^3$ kg/ m^3

Table 3 Parameter *b* employed for different poroelastic systems

	First layer, $b^{(1)}$	Second layer, $b^{(2)}$	Half-space, $b^{(3)}$
System PA	$6.32\text{x}10^2$	$6.32\text{x}10^2$	$6.32\text{x}10^2$
System PB	$1.5\text{x}10^6$	$7.5\text{x}10^6$	$4.5\text{x}10^6$

$N\,s/m^4$

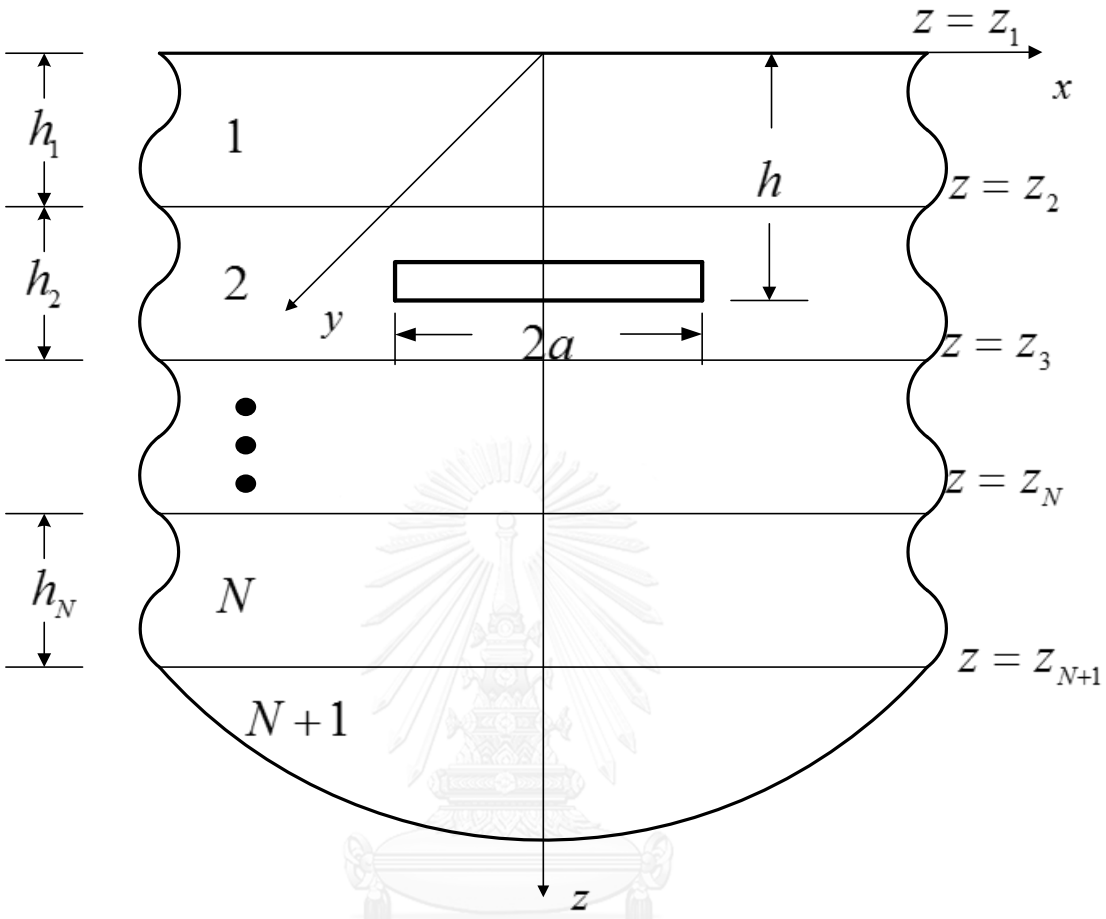

Figure 1 A rigid plate embedded in a multi-layered poroelastic half-space

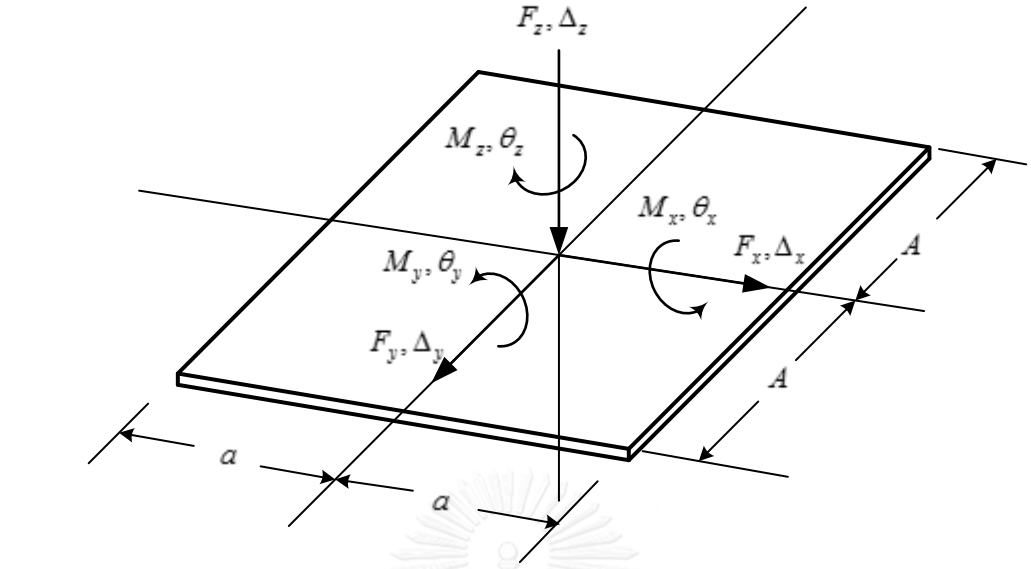

(a)

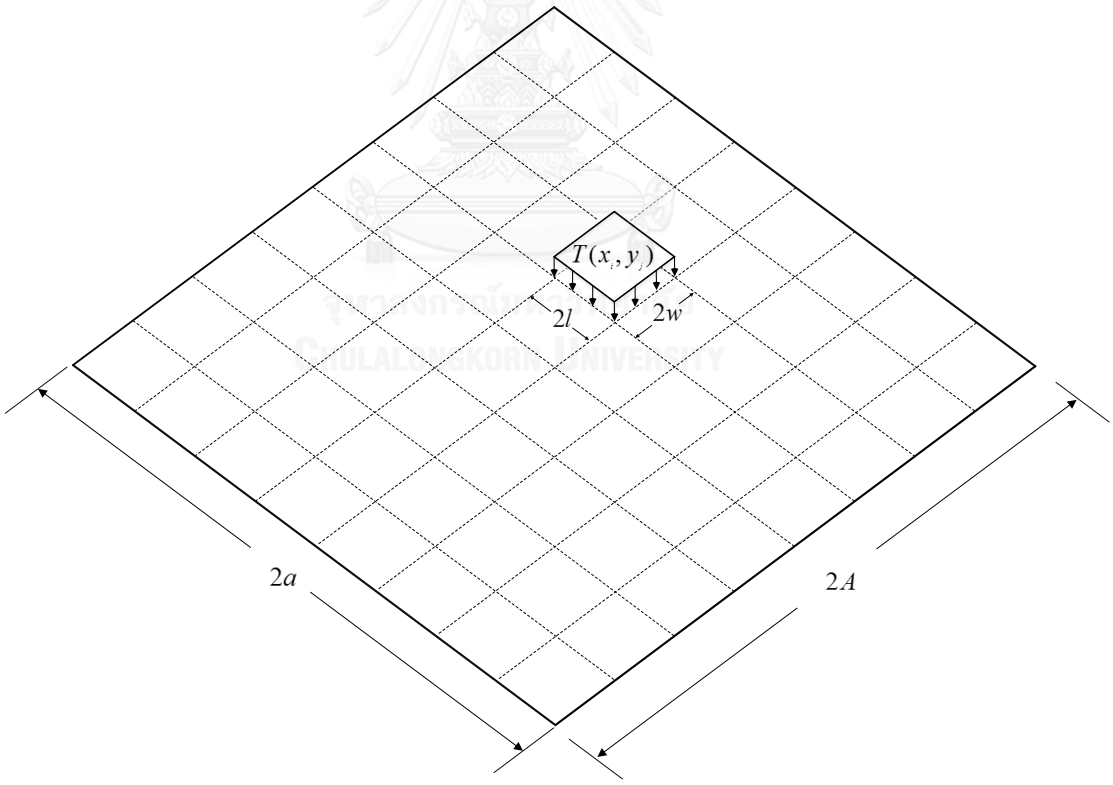

(b)

Figure 2 A rectangular plate under loading; and discretization of contact area

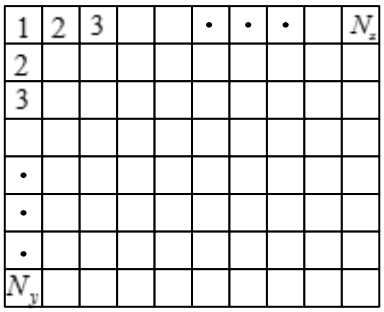

(a)

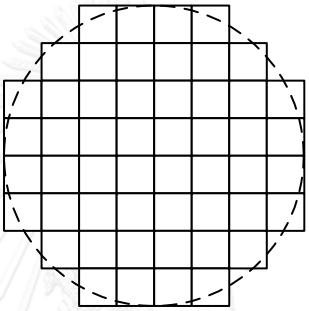

(b)

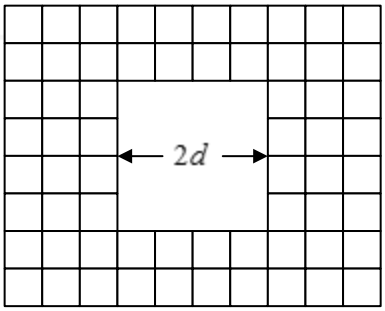

(c)

Figure 3 Discretization of plates: (a) rectangular plate; (b) circular plate; (c) rectangular plate with square hole

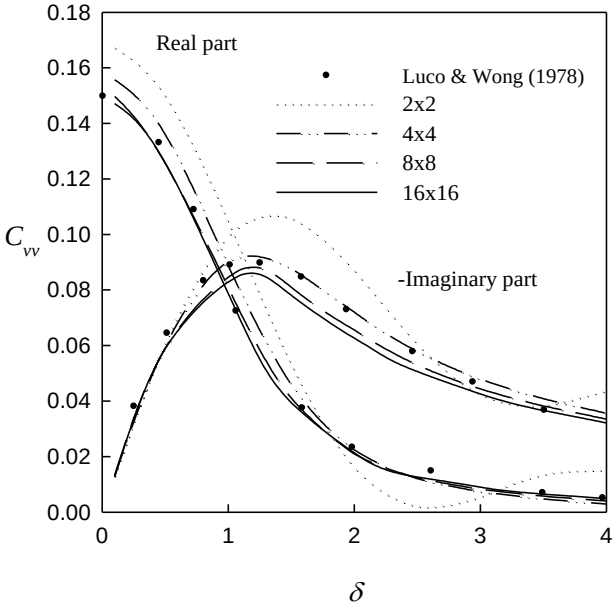

(a)

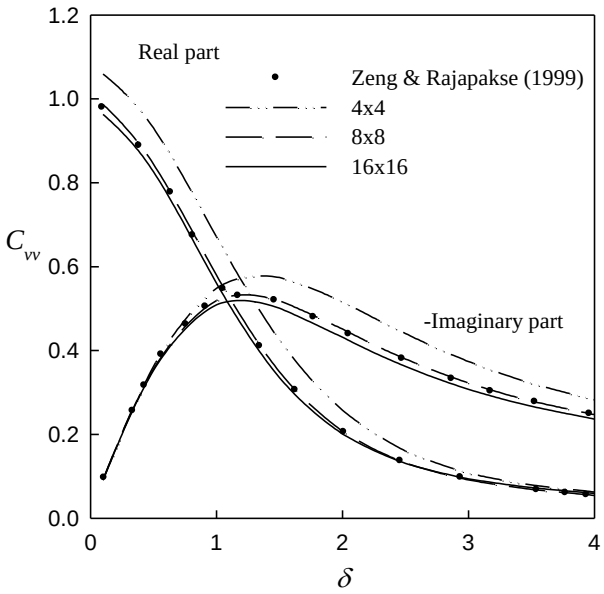

(b)

Figure 4 Convergence and accuracy of present solution: (a) elastic half-space; (b) poroelastic half-space

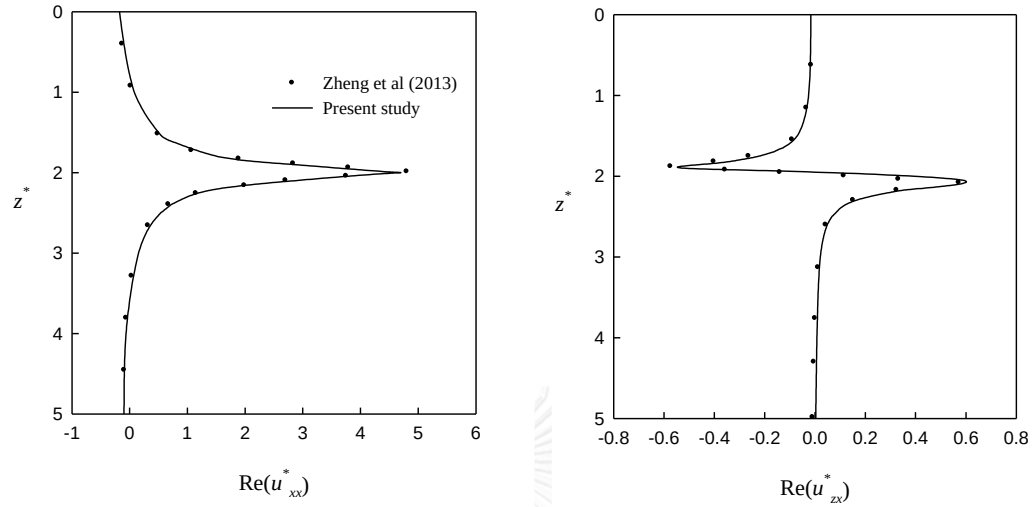

(a)

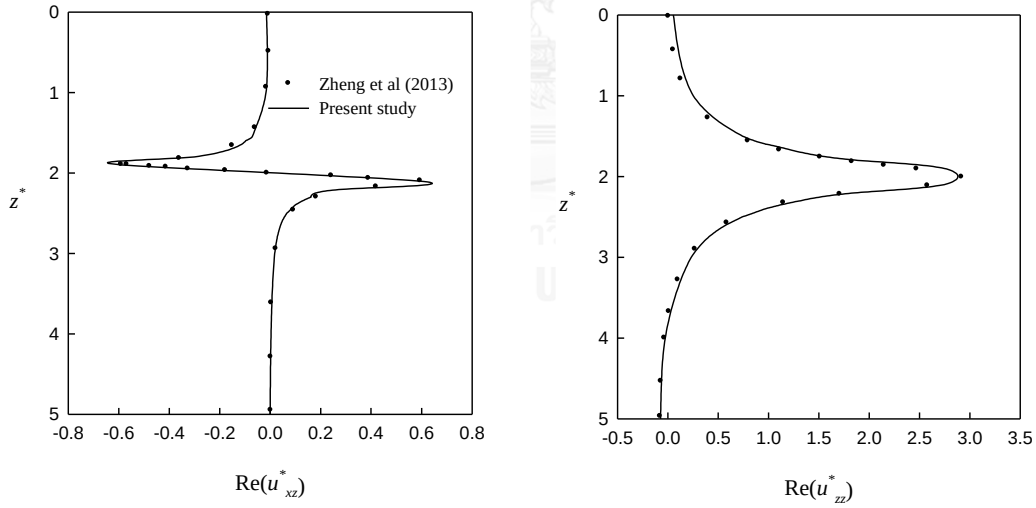

(b)

Figure 5 Comparison of displacements along the z -axis of homogenous poroelastic half-space under (a) horizontal loading; (b) vertical loading

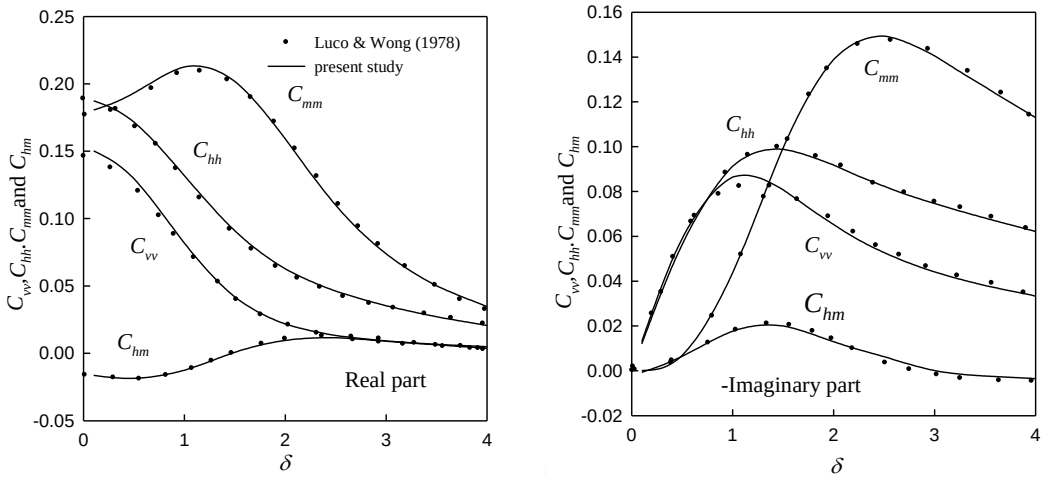

(a)

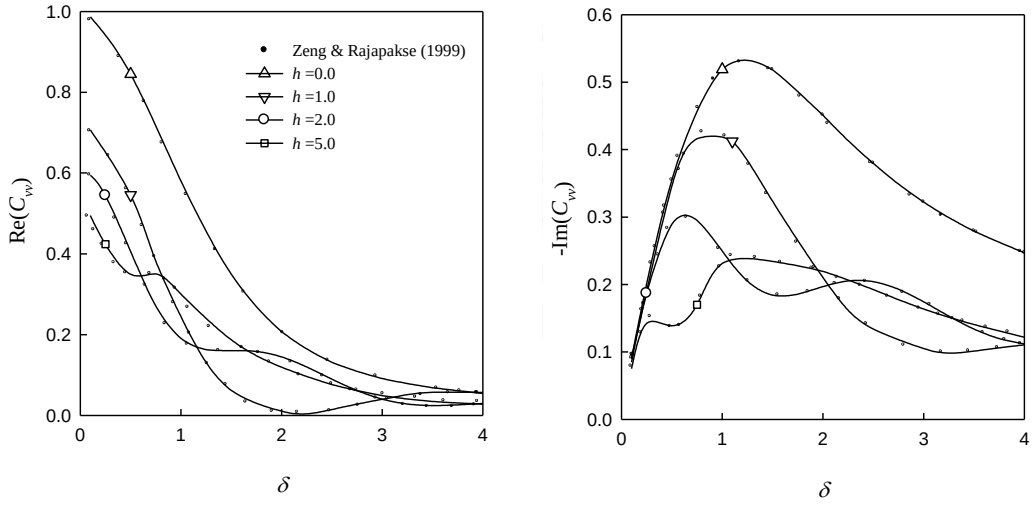

(b)

Figure 6 Comparison of compliances for (a) elastic half-space; (b) poroelastic half-space

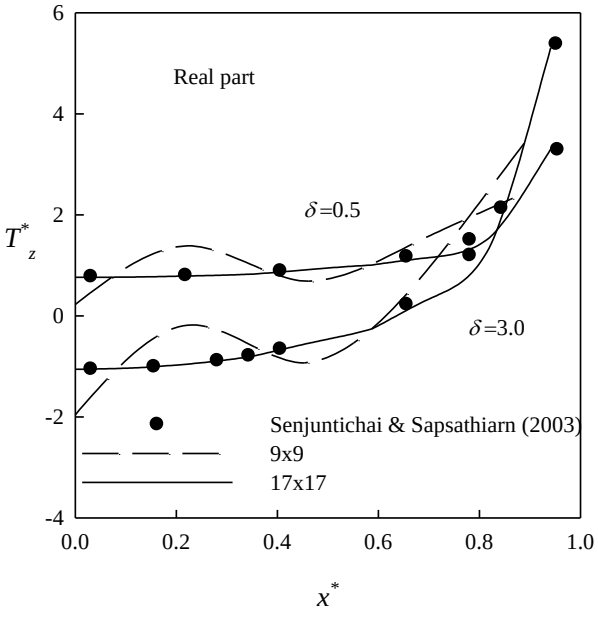

(a)

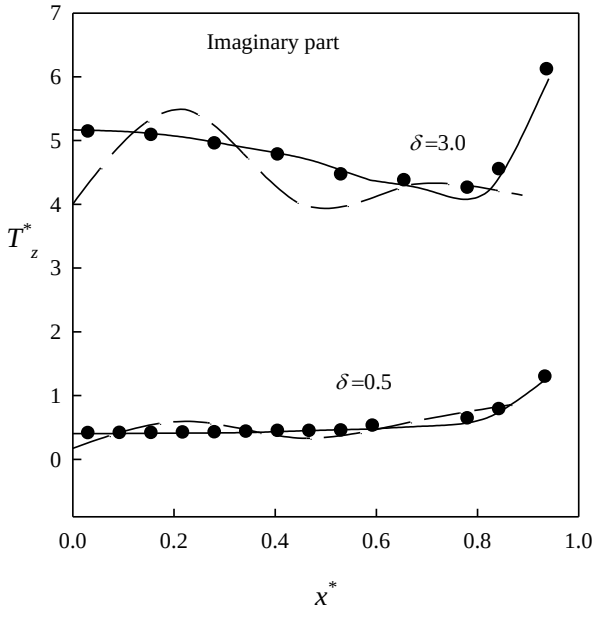

(b)

Figure 7 Comparison of traction profiles along the radius of circular plate

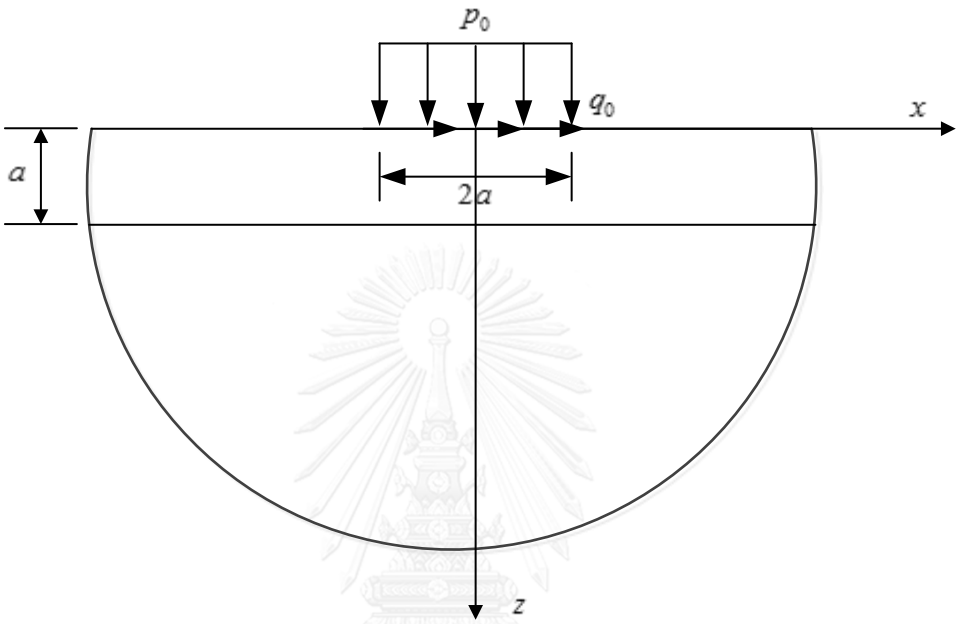

Figure 8 A layered poroelastic half-space under surface loading

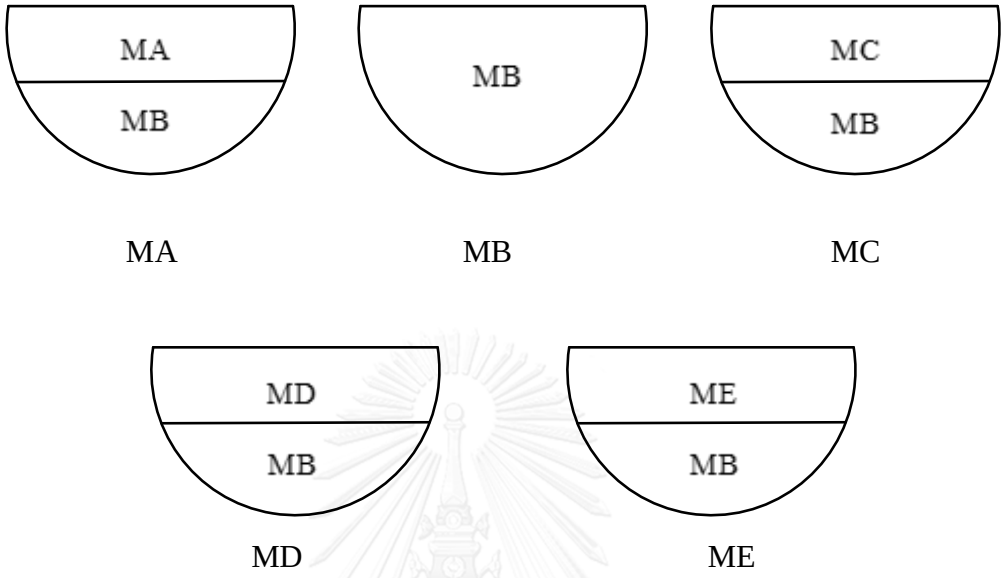

Figure 9 Five cases of two-layered systems considered in the numerical study

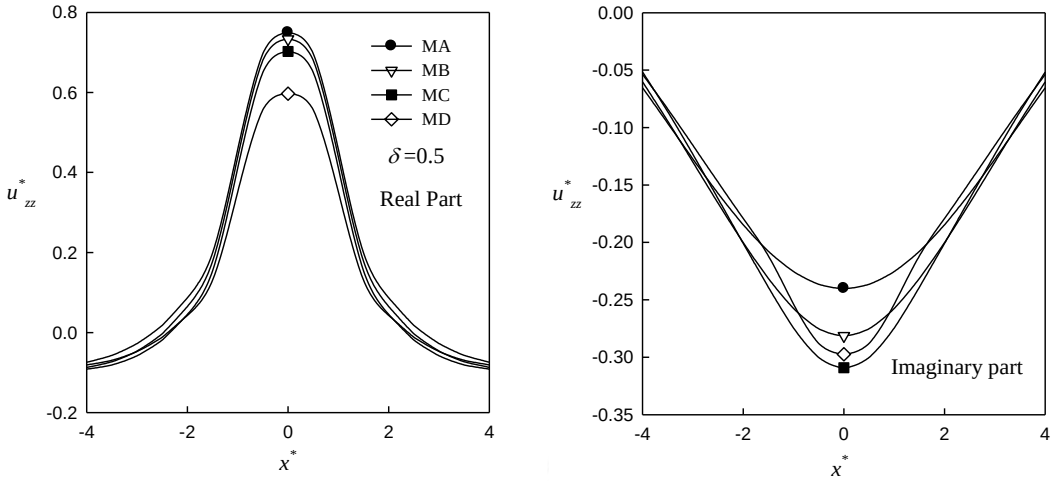

(a)

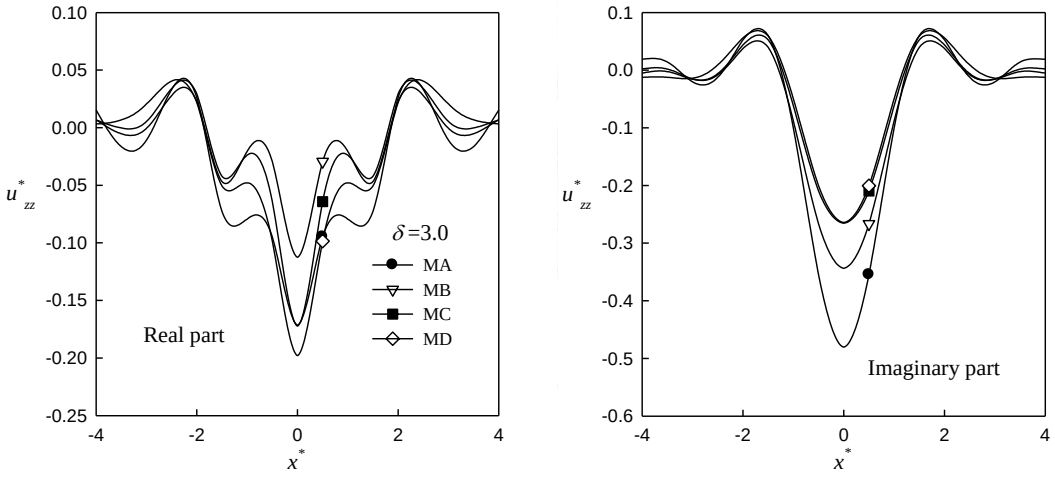

(b)

Figure 10 The vertical displacement along the x-axis due to the vertical loading: (a) $\delta = 0.5$; (b) $\delta = 3.0$

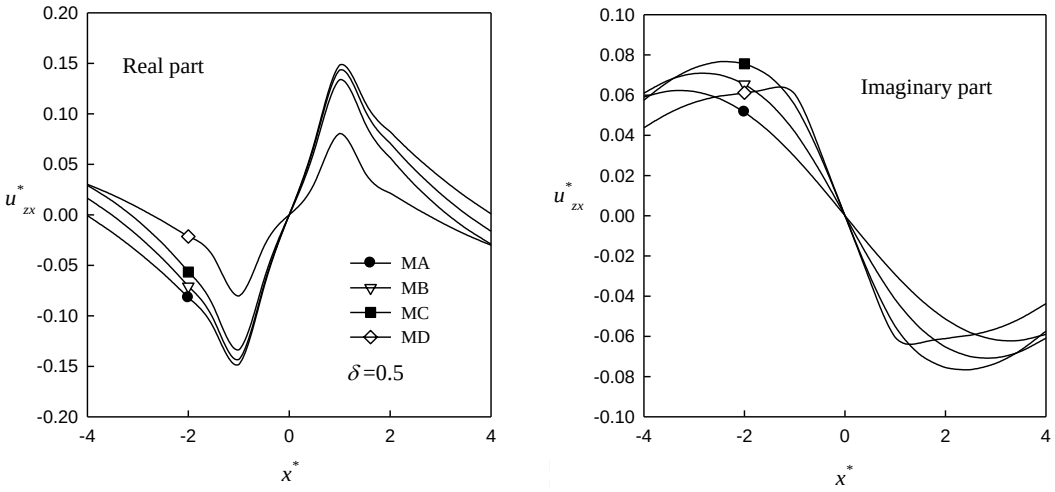

(a)

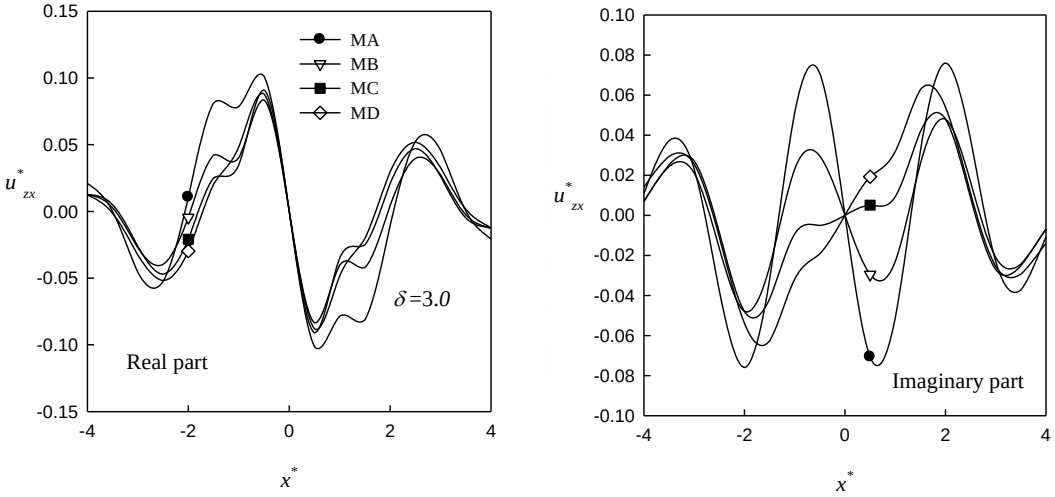

(b)

Figure 11 The vertical displacement along the x-axis due to the horizontal loading: (a) $\delta = 0.5$; (b) $\delta = 3.0$

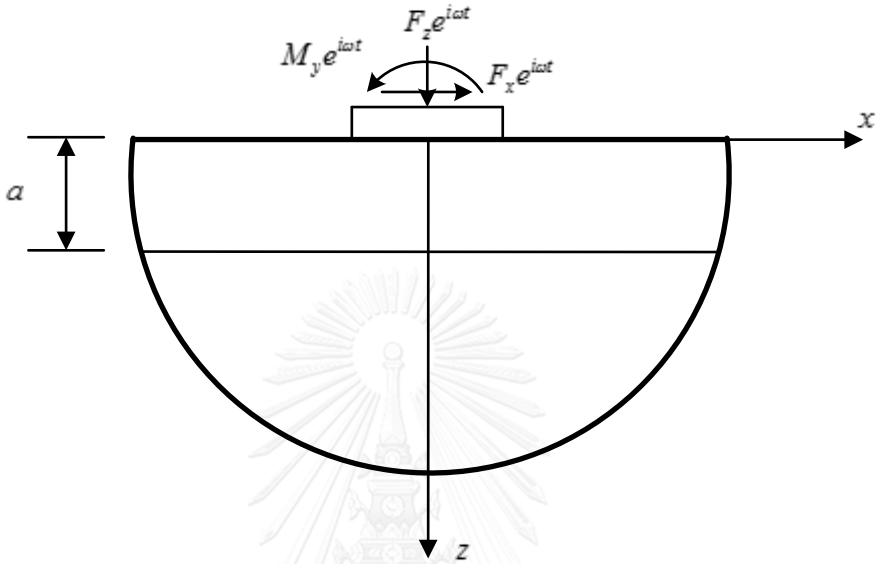

Figure 12 A rigid rectangular plate on a two-layered poroelastic system

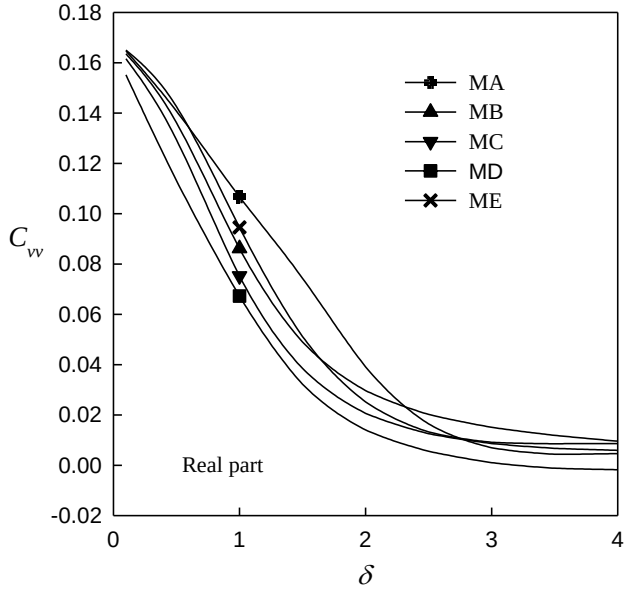

(a)

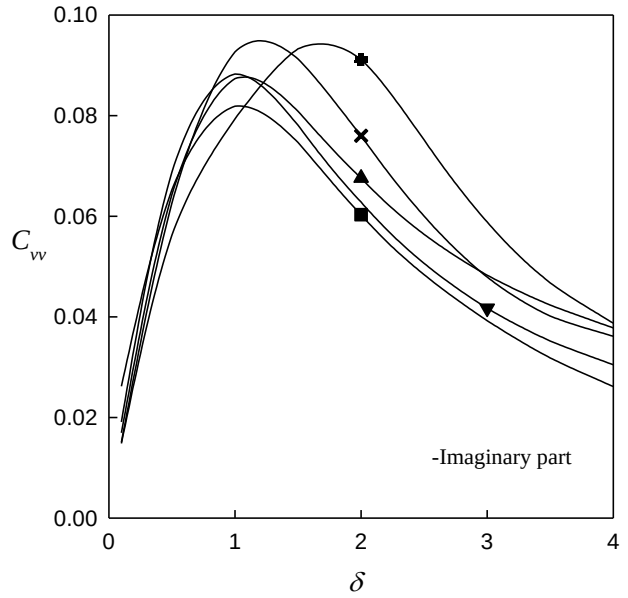

(b)

Figure 13 The vertical compliances for different layered poroelastic media

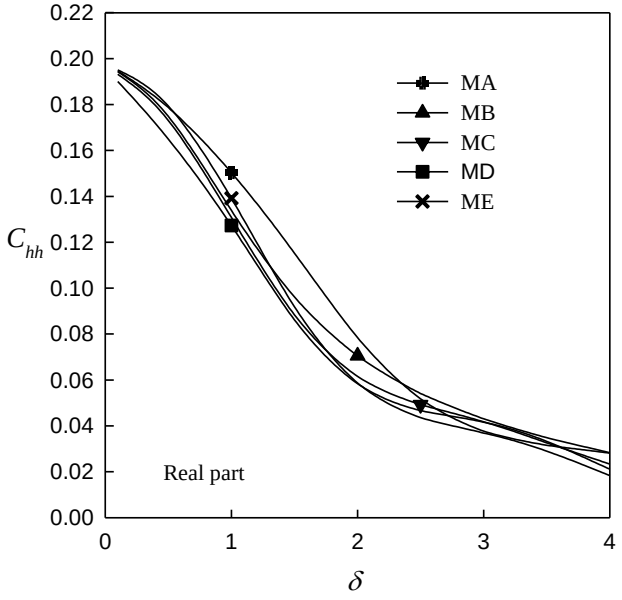

(a)

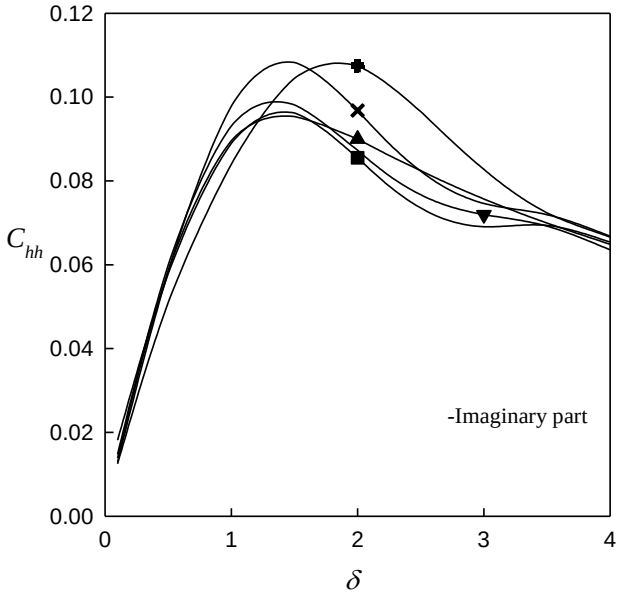

(b)

Figure 14 The horizontal compliances for different layered poroelastic media

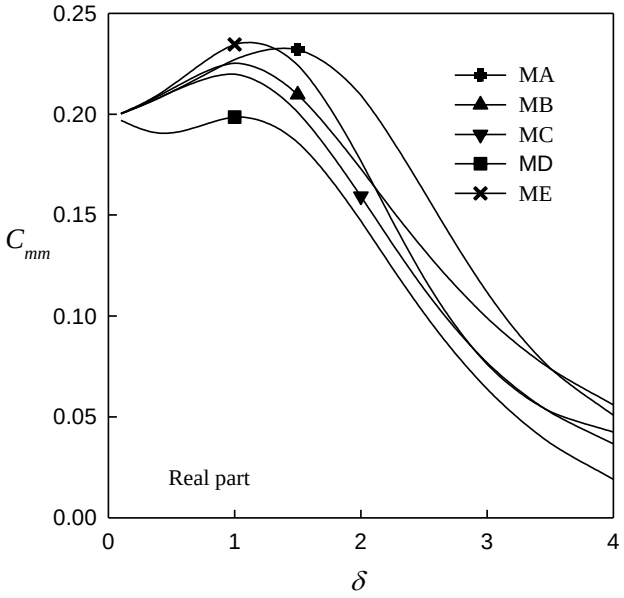

(a)

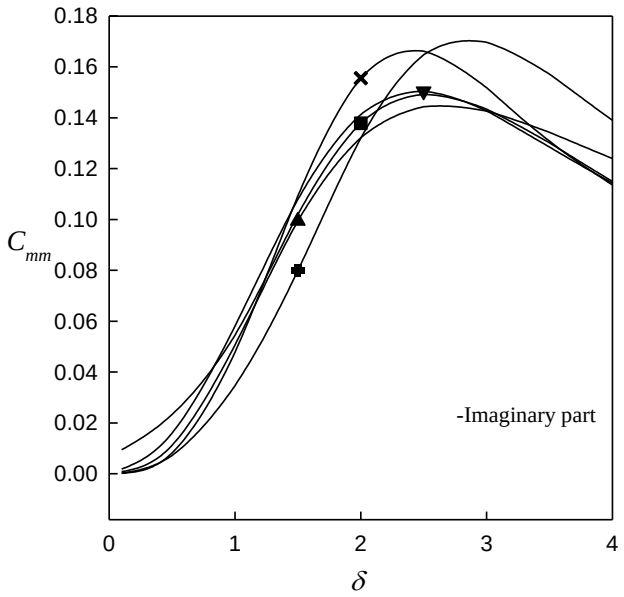

(b)

Figure 15 The rocking compliances for different layered poroelastic media

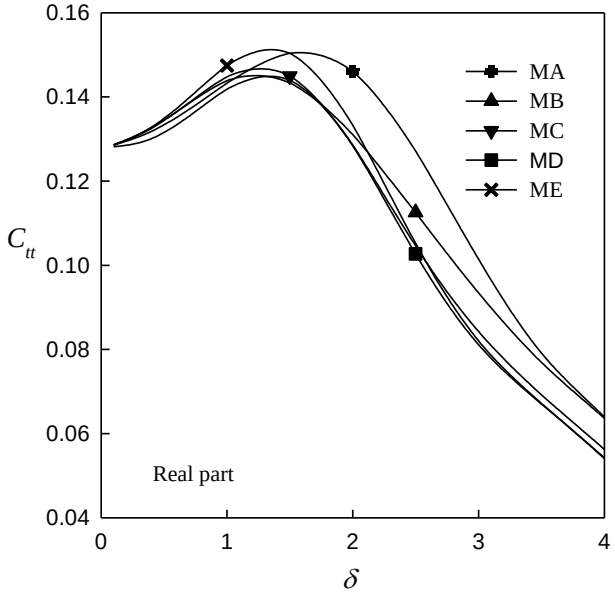

(a)

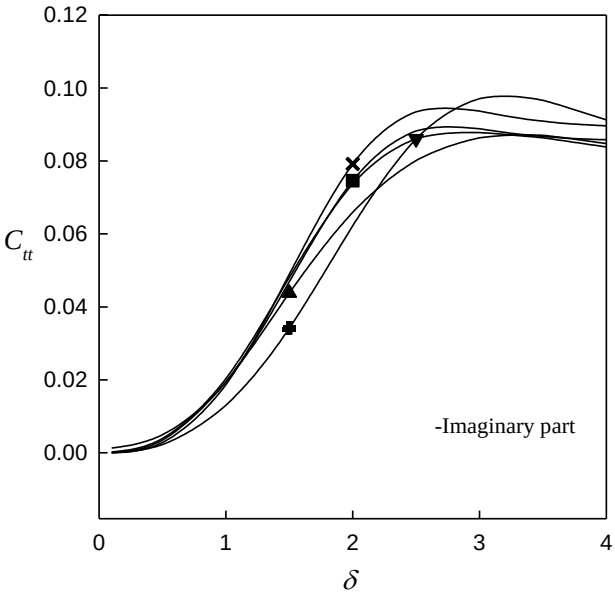

(b)

Figure 16 The torsion compliances for different layered poroelastic media

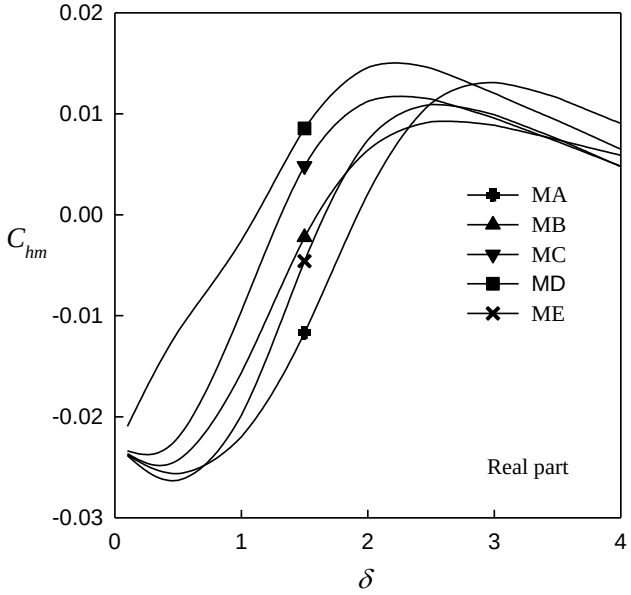

(a)

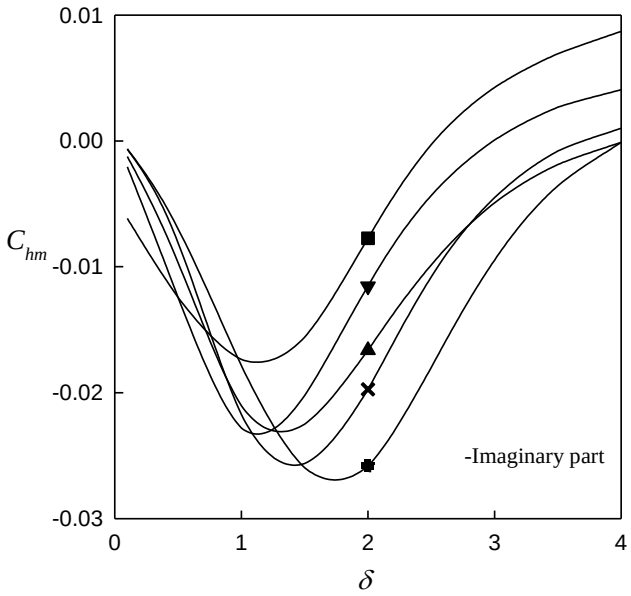

(b)

Figure 17 The coupling compliances for different layered poroelastic media

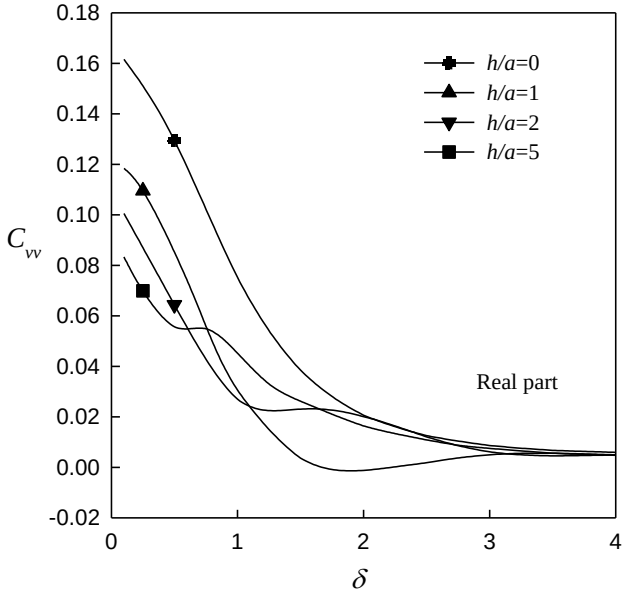

(a)

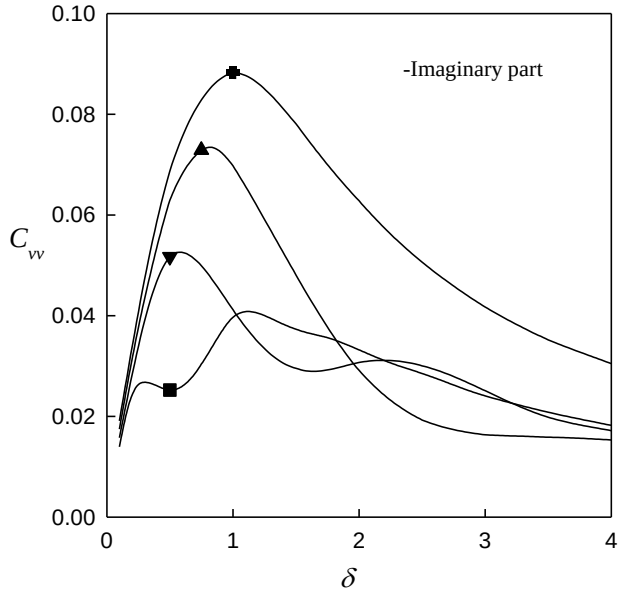

(b)

Figure 18 The vertical compliances for different embedded depths (h/a)

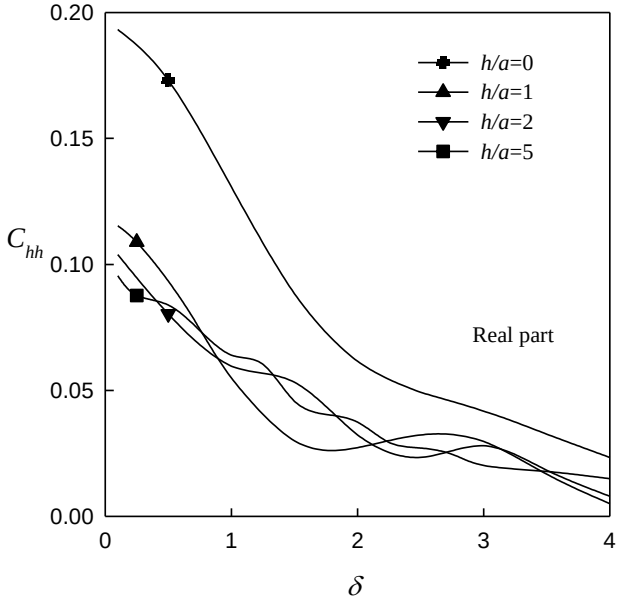

(a)

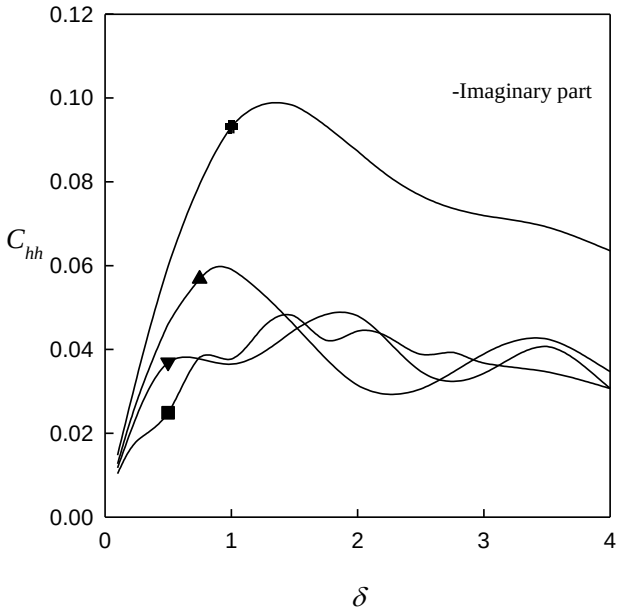

(b)

Figure 19 The horizontal compliances for different embedded depths (h/a)

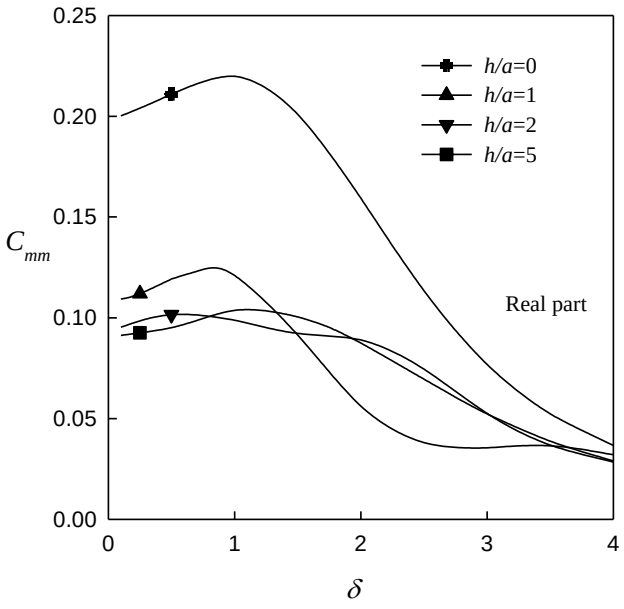

(a)

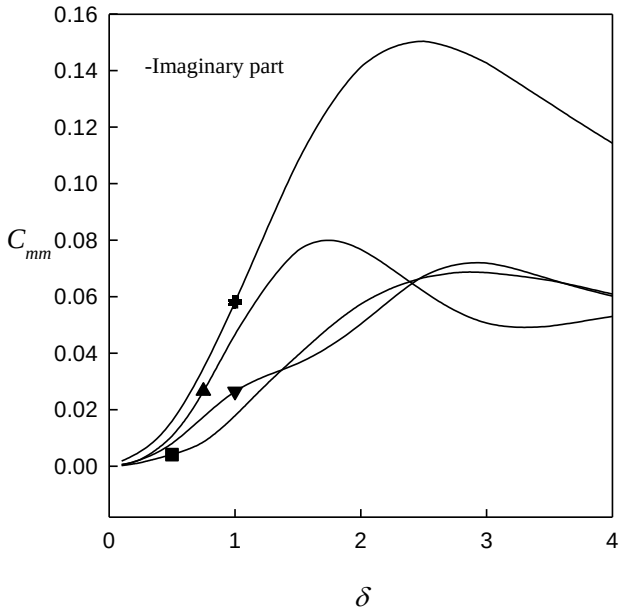

(b)

Figure 20 The rocking compliances for different embedded depths (h/a)

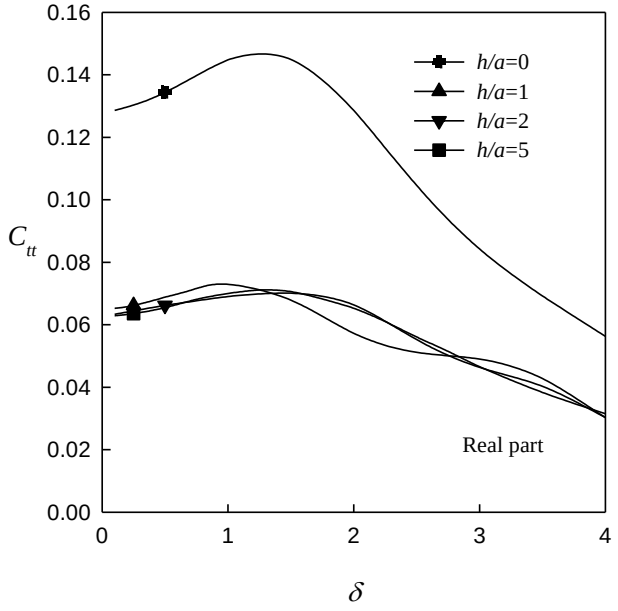

(a)

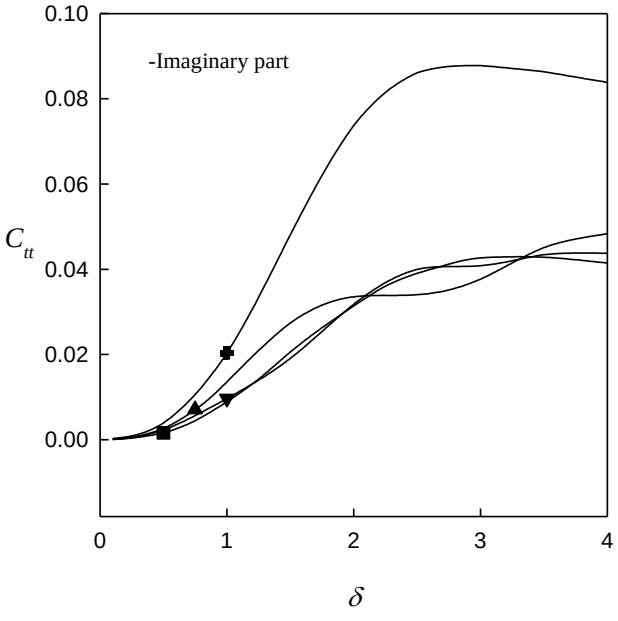

(b)

Figure 21 The torsion compliances for different embedded depths (h/a)

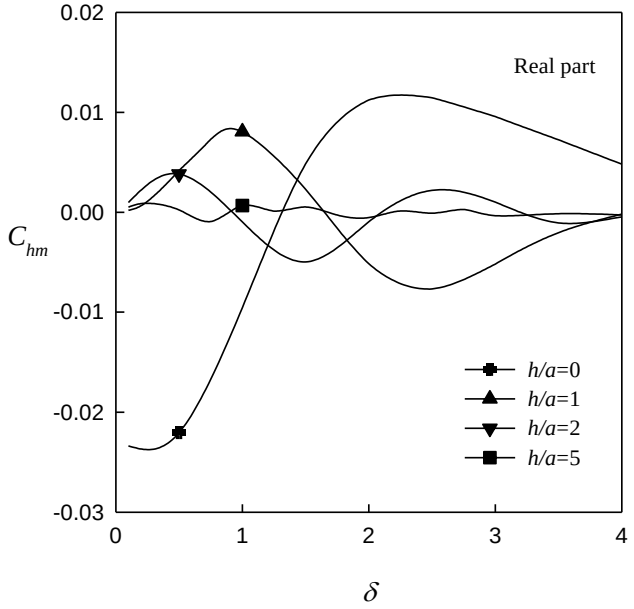

(a)

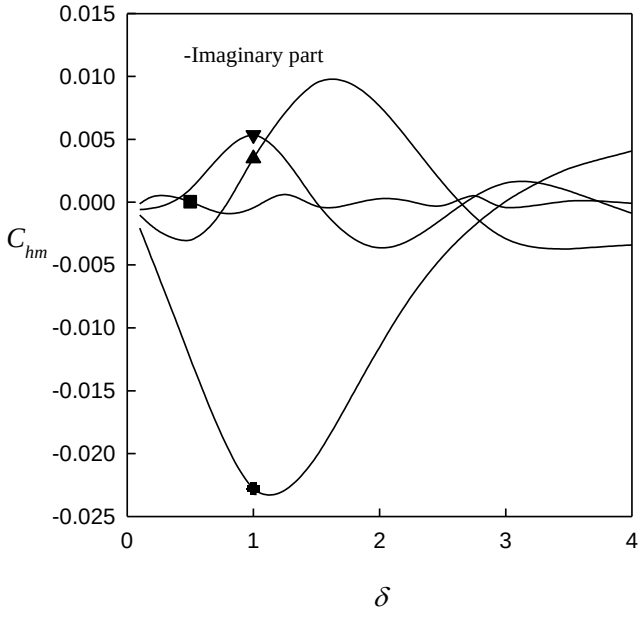

(b)

Figure 22 The coupling compliances for different embedded depths (h/a)

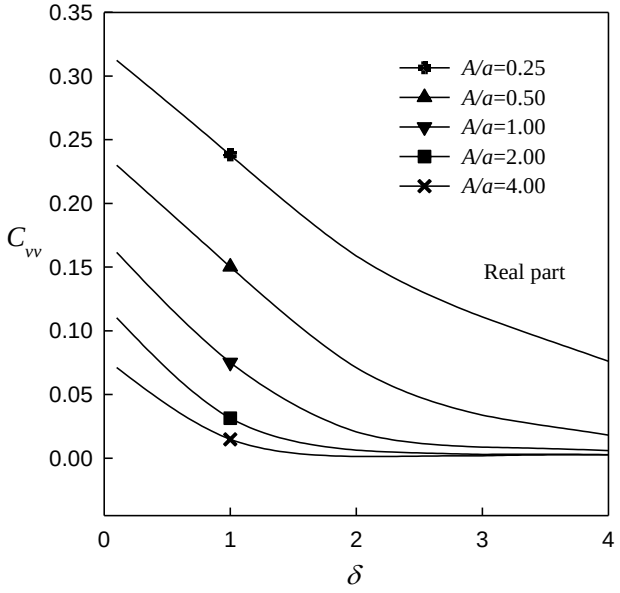

(a)

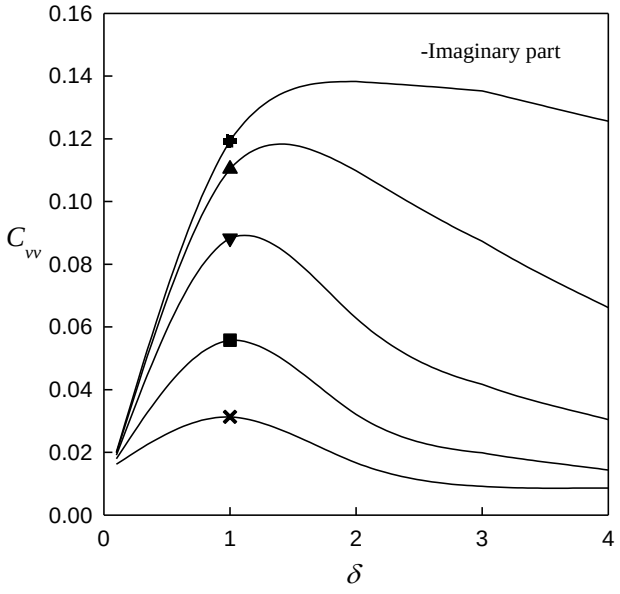

(b)

Figure 23 The vertical compliances for different aspect ratios of plate (A/a)

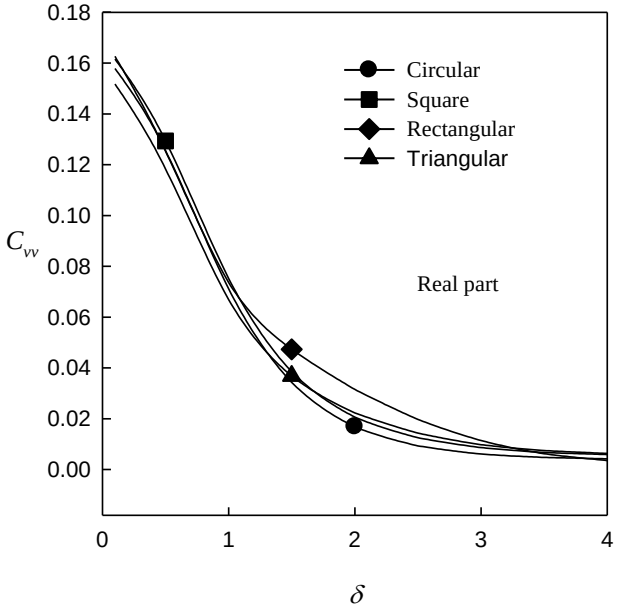

(a)

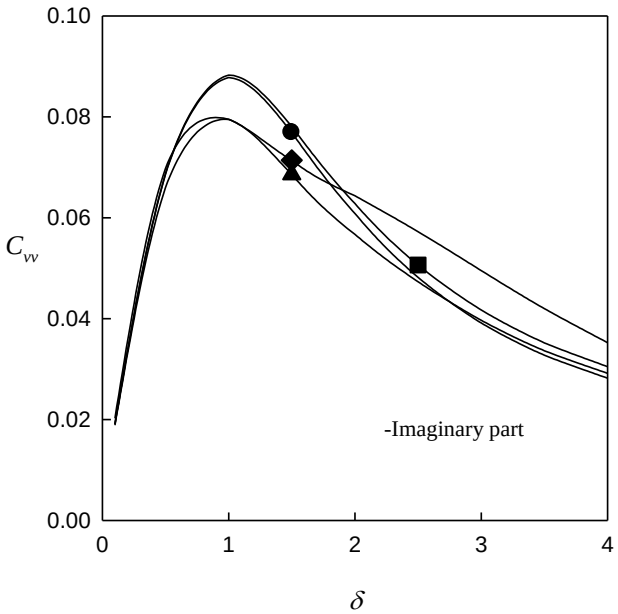

(b)

Figure 24 The vertical compliances for plates of various shapes (A/a)

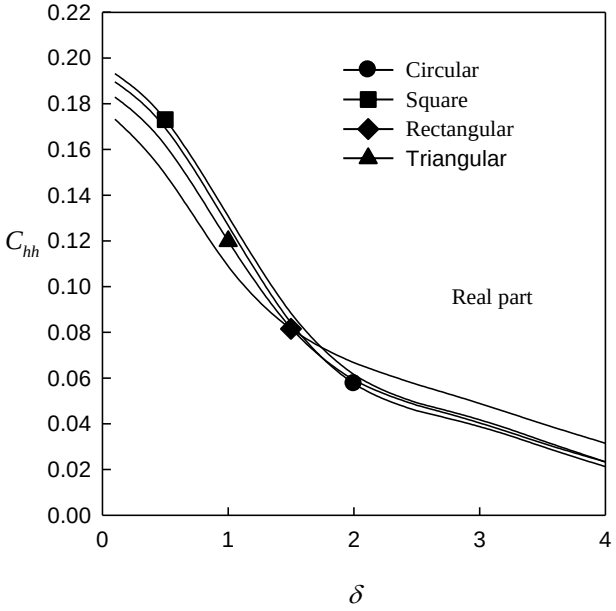

(a)

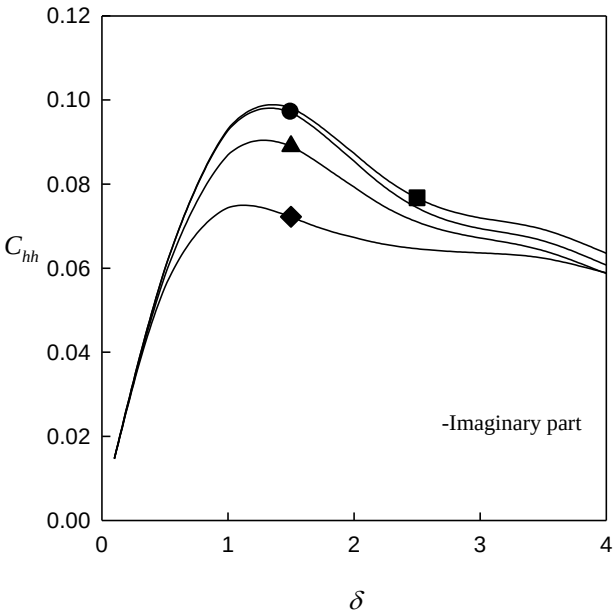

(b)

Figure 25 The horizontal compliances for plates of various shapes (A/a)

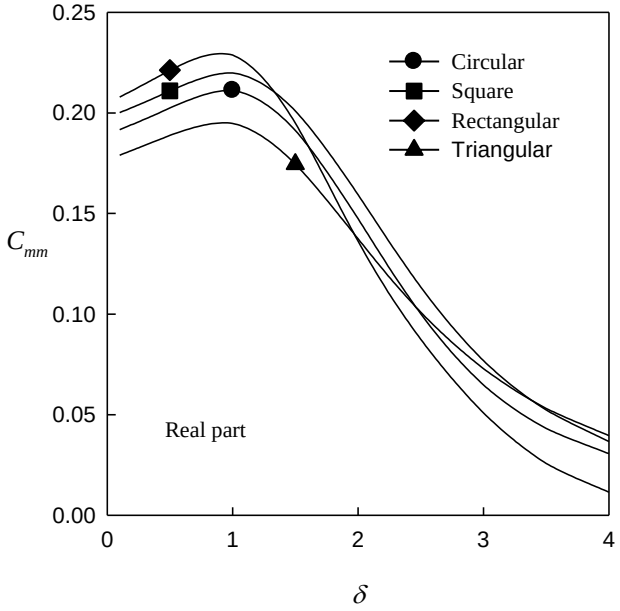

(a)

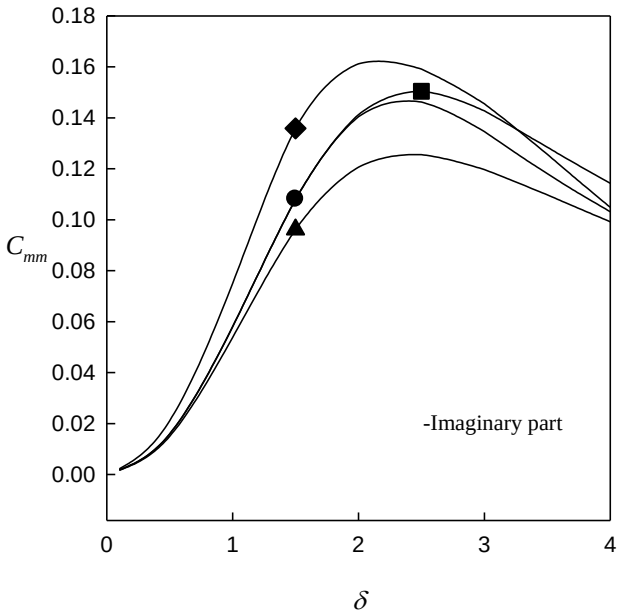

(b)

Figure 26 The rocking compliances for plates of various shapes (A/a)

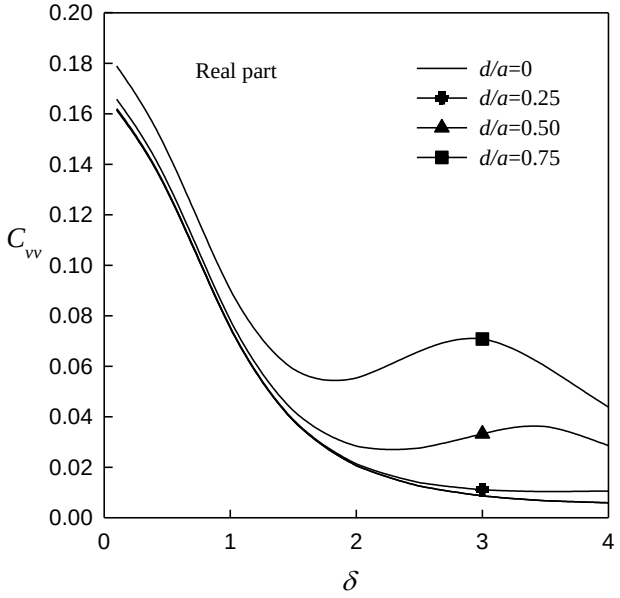

(a)

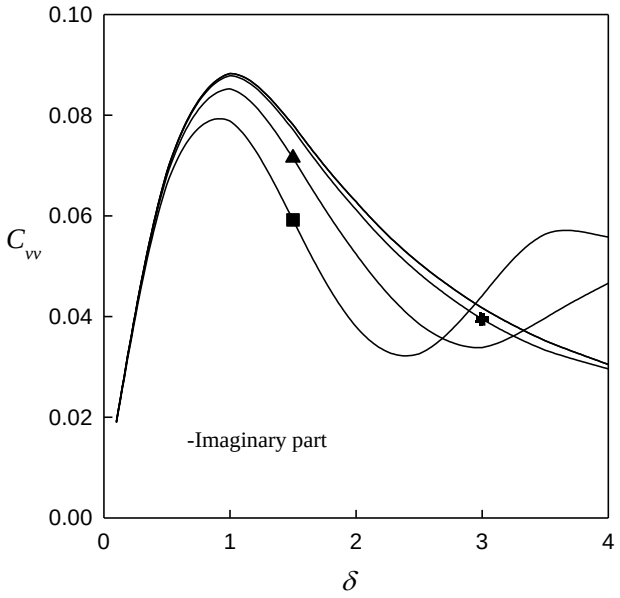

(b)

Figure 27 The vertical compliances for rectangular plate with square hole (d/a)

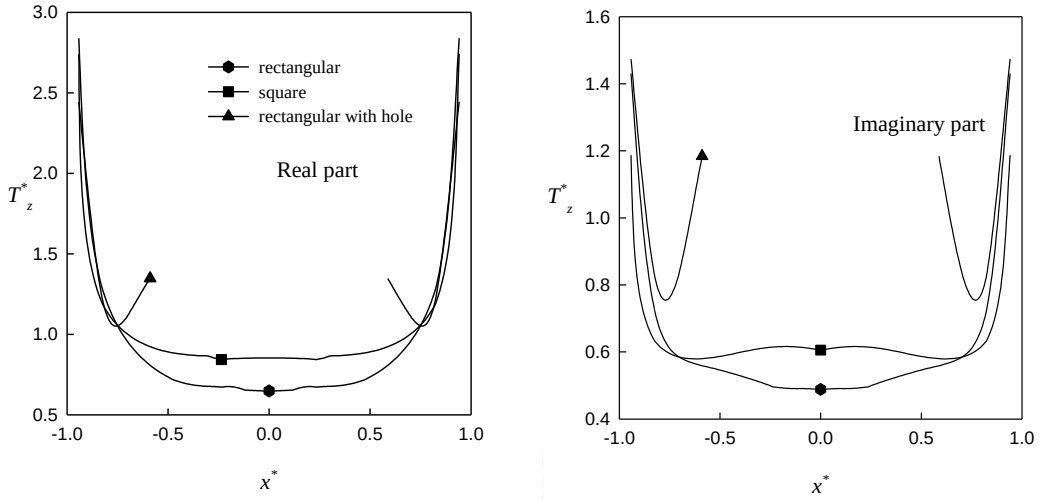

(a)

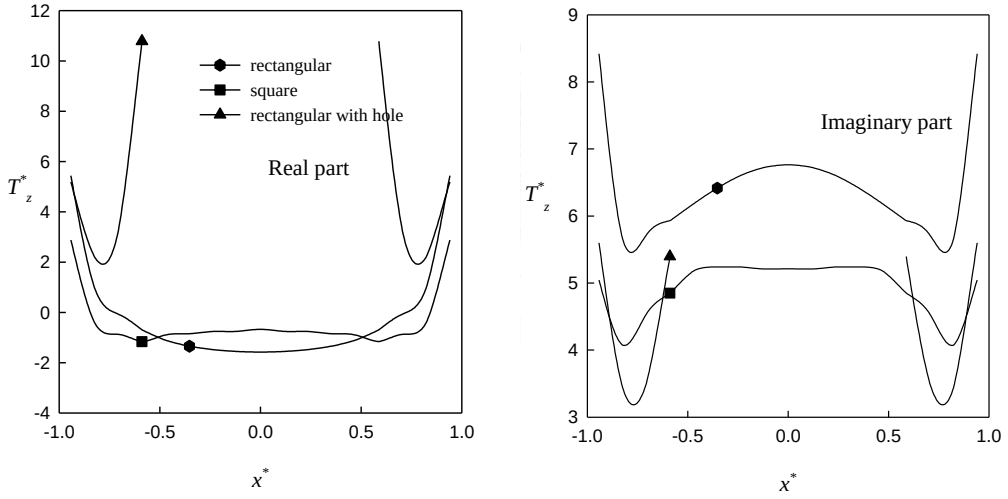

(b)

Figure 28 The traction profiles along the center line of plates

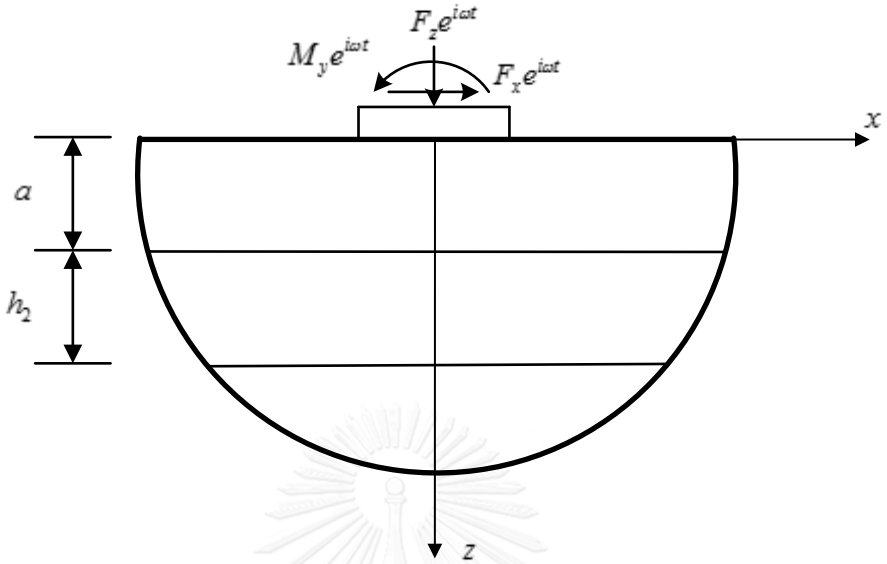

Figure 29 A rigid rectangular plate on a three-layered poroelastic system

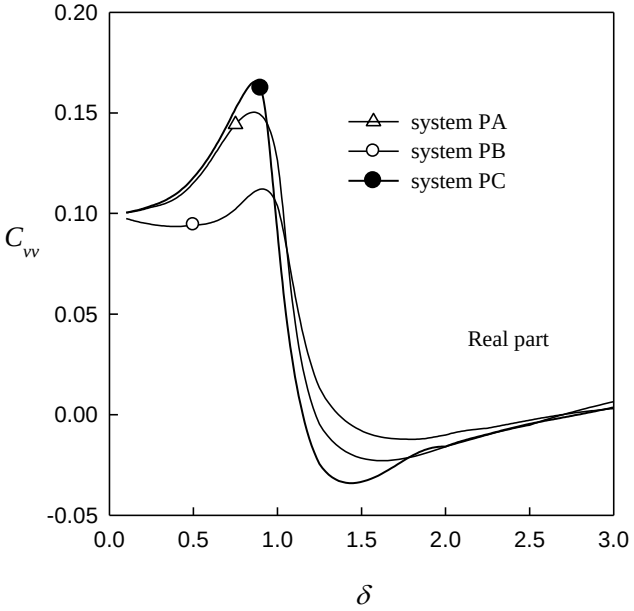

(a)

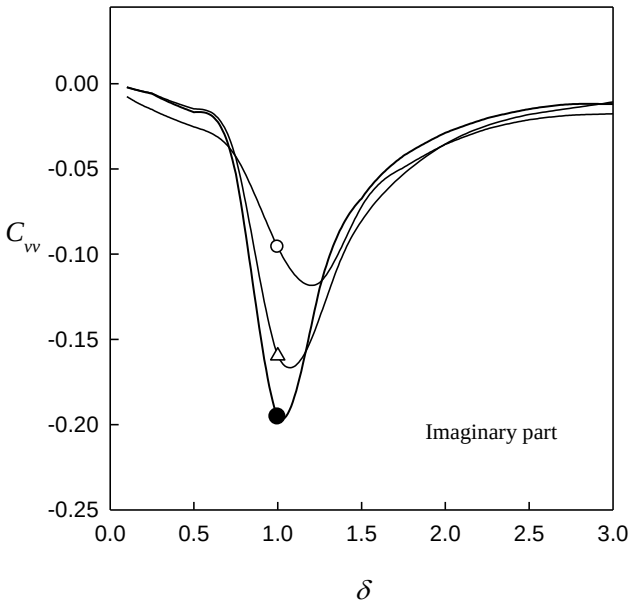

(b)

Figure 30 The verical comliances for different three-layered systems

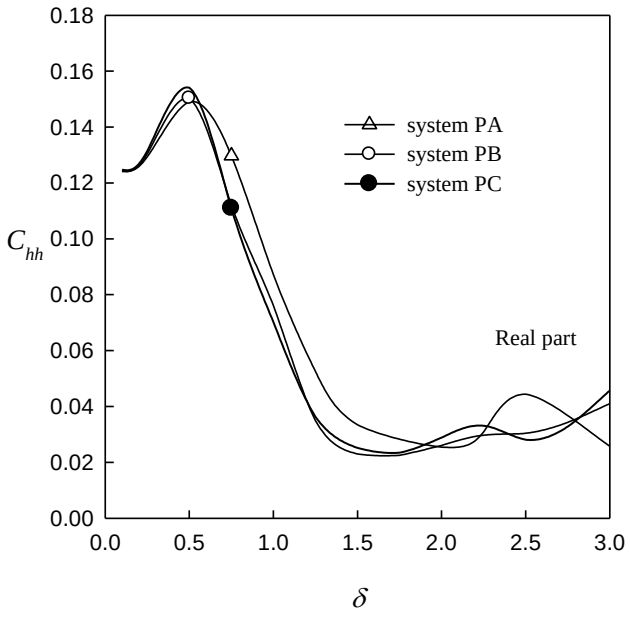

(a)

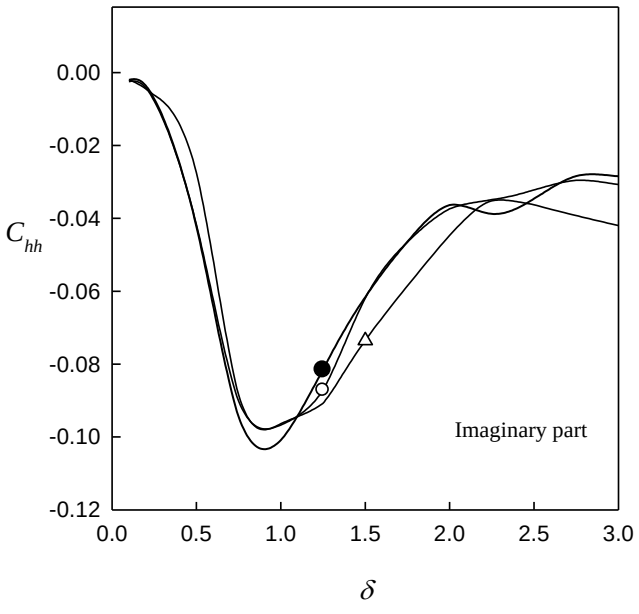

(b)

Figure 31 The horizontal comliances for different three-layered systems

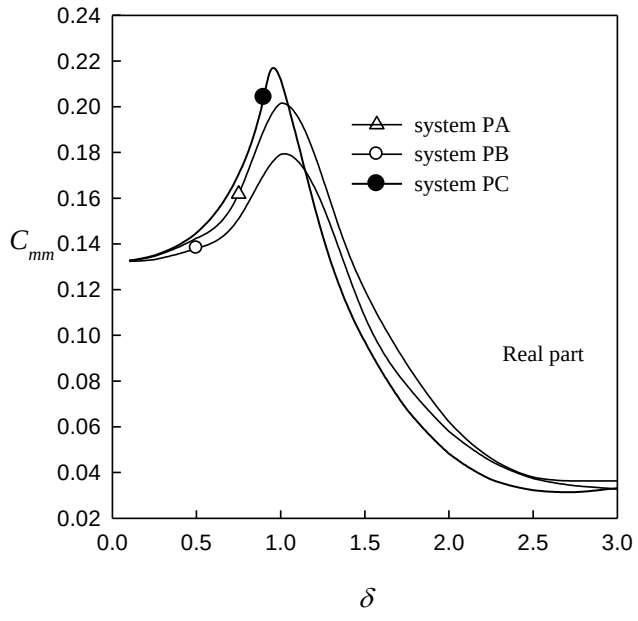

(a)

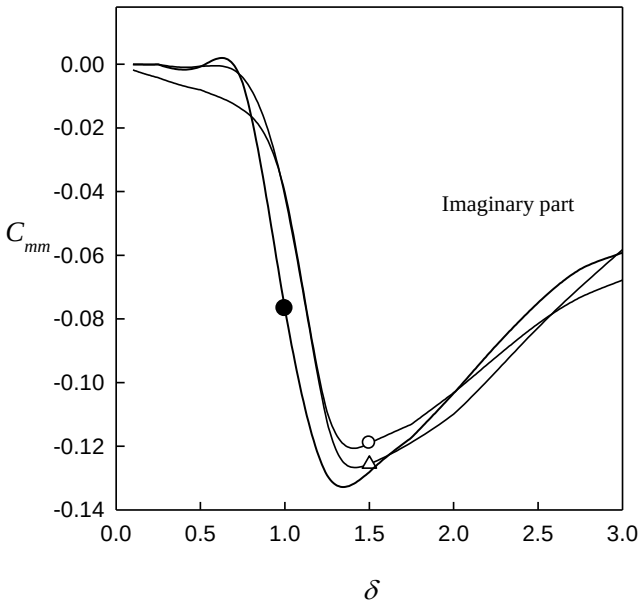

(b)

Figure 32 The rocking comliances for different three-layered systems

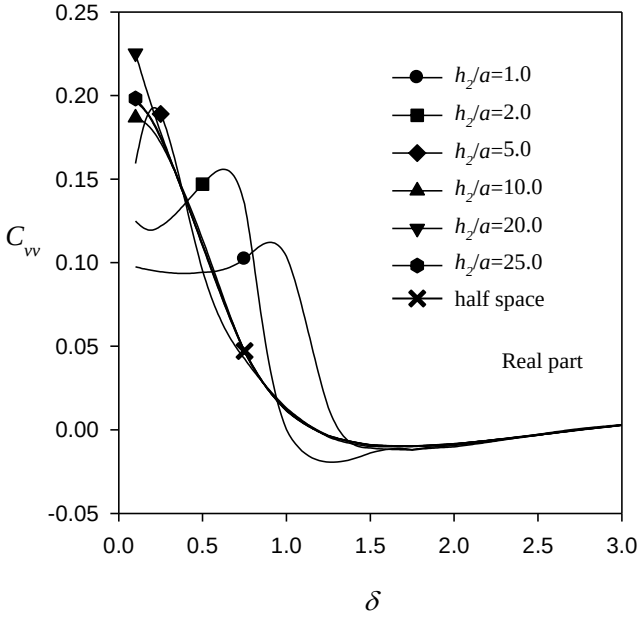

(a)

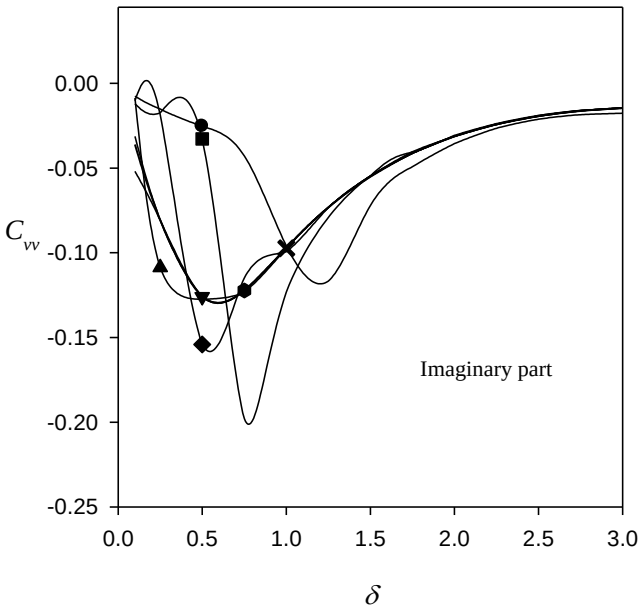

(b)

Figure 33 The vertical compliances for different thicknesses of the second layer $\left(h_2 / a\right)$

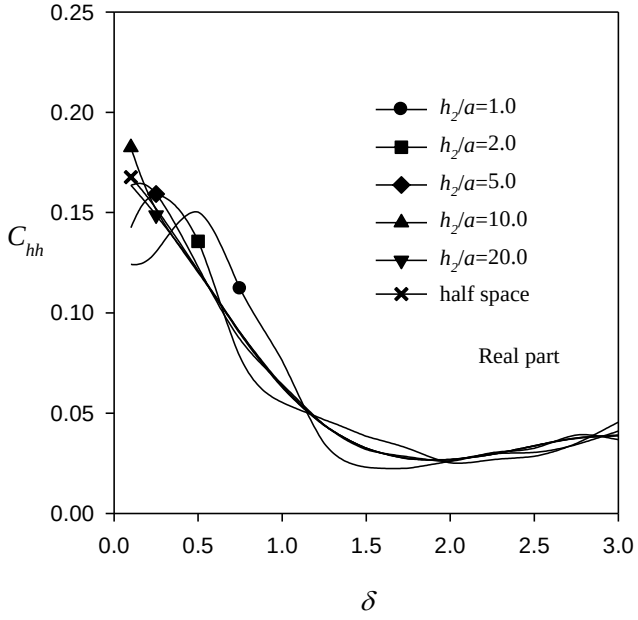

(a)

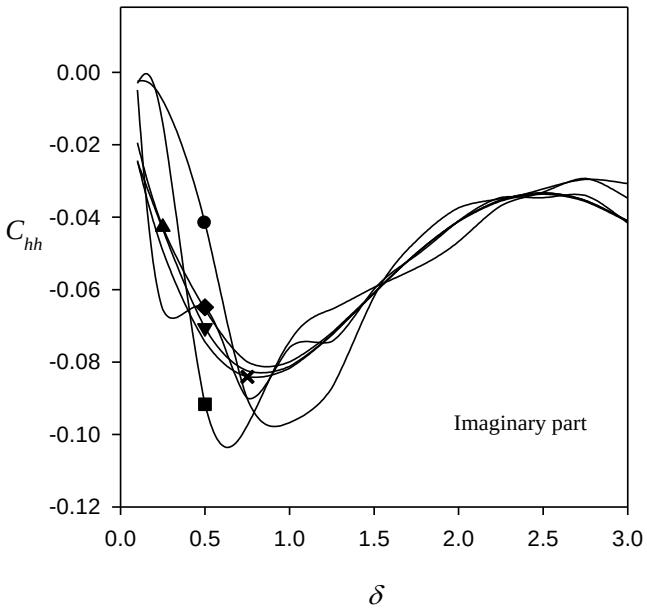

(b)

Figure 34 The horizontal compliances for different thicknesses of the second layer $\left(h_2 / a\right)$

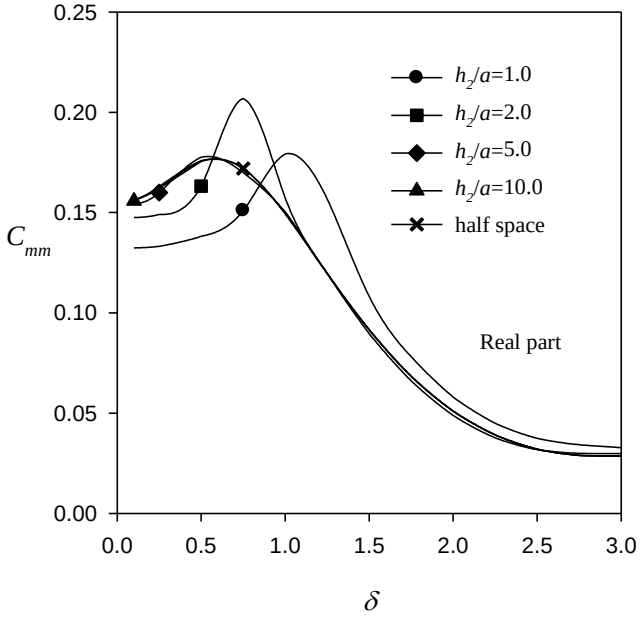

(a)

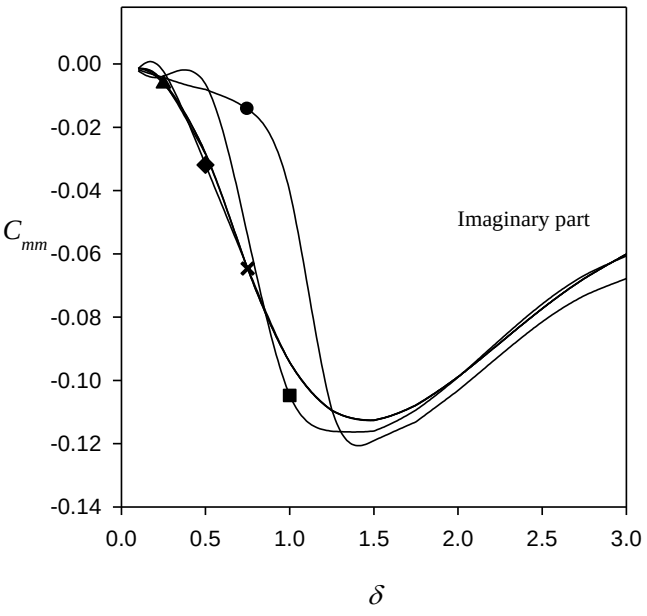

(b)

Figure 35 The rocking compliances for different thicknesses of the second layer $\left(h_2 / a\right)$

VITA

Mr. Rawiphas Plangmal was born on February 1, 1992 in Mahasarakham Province, Thailand. He obtained his bachelor degree in civil engineering from the faculty of engineering, Khon Kaen University in 2014. He later pursued his study in the master program in Civil Engineering at Chulalongkorn University in 2014.